Mon. Not. R. Astron. Soc. **360,** 1455–1470 (2005) doi:10.1111/j.1365-2966.2005.09143.x

Unusual high-redshift radio broad absorption-line quasar 1624+3758

C. R. Benn,[1★] R. Carballo,[2] J. Holt,[3] M. Vigotti,[4] J. I. González-Serrano,[5] K.-H. Mack[4] and R. A. Perley[6]

[1] *Isaac Newton Group, Apartado 321, E-38700 Santa Cruz de La Palma, Spain*
[2] *Departamento de Matemática Aplicada y C. Computación, Universidad de Cantabria, E-39005 Santander, Spain*
[3] *Department of Physics & Astronomy, University of Sheffield, Hicks Building, Sheffield S3 7RH*
[4] *Istituto di Radioastronomia, CNR, via Gobetti 101, I-40129 Bologna, Italy*
[5] *Instituto de Física de Cantabria (CSIC-UC), Facultad de Ciencias, E-39005 Santander, Spain*
[6] *National Radio Astronomy Observatory, PO Box 0, Socorro, NM 87801, USA*

Accepted 2005 April 18. Received 2005 March 14; in original form 2005 February 2

ABSTRACT

We present observations of the most radio-luminous broad absorption-line (BAL) quasar known, 1624+3758, at redshift $z = 3.377$. The quasar has several unusual properties. (1) The Fe II UV191 1787-Å emission line is very prominent. (2) The BAL trough (BALnicity index 2990 km s^{-1}) is detached by 21 000 km s^{-1} and extends to velocity $v = -29\,000$ km s^{-1}. There are additional intrinsic absorbers at −1900 and −2800 km s^{-1}. (3) The radio rotation measure of the quasar, 18 350 rad m^{-2}, is the second highest known. The radio luminosity is $P_{1.4\,\mathrm{GHz}} = 4.3 \times 10^{27}$ W Hz^{-1} ($H_0 = 50$ km s^{-1} Mpc^{-1}, $q_0 = 0.5$) and the radio loudness is $R^* = 260$. The radio source is compact ($\gtrsim$2.8 kpc) and the radio spectrum is GHz-peaked, consistent with it being relatively young. The width of the C IV emission line, in conjunction with the total optical luminosity, implies a black hole mass $M_{\mathrm{BH}} \sim 10^9\,\mathrm{M}_{\odot}$, $L/L_{\mathrm{Eddington}} \approx 2$. The high Eddington ratio and the radio-loudness place this quasar in one corner of Boroson's two-component scheme for the classification of active galactic nuclei, implying a very high accretion rate, and this may account for some of the unusual observed properties. The $v = -1900$ km s^{-1} absorber is a possible Lyman-limit system, with $N(\mathrm{H\,I}) = 4 \times 10^{18}$ cm^{-2}, and a covering factor of 0.7. A complex mini-BAL absorber at $v = -2200$ to -3400 km s^{-1} is detected in each of C IV, N V and O VI. The blue and red components of the C IV doublet happen to be unblended, allowing both the covering factor and optical depth to be determined as a function of velocity. Variation of the covering factor with velocity dominates the form of the mini-BAL, with the absorption being saturated ($e^{-\tau} \approx 0$) over most of the velocity range. The velocity dependence of the covering factor and the large velocity width imply that the mini-BAL is intrinsic to the quasar. There is some evidence of line-locking between velocity components in the C IV mini-BAL, suggesting that radiation pressure plays a role in accelerating the outflow.

Key words: galaxies: high-redshift – intergalactic medium – quasars: absorption lines – quasars: emission lines – quasars: general – early Universe.

1 INTRODUCTION

In 10–20 per cent of optically selected quasars, broad absorption lines (BALs) are seen in the blue wings of the ultraviolet (UV) resonance emission lines (e.g. C IV), due to gas with outflow velocities up to ∼0.2c (Hewett & Foltz 2003). The absorption troughs can be highly structured, but are smooth compared with thermal linewidths. Approximately 20 per cent of BALs are detached from the corresponding emission line by several thousand km s^{-1} (see Korista et al. 1993 for examples). The blue and red edges of the BAL absorption trough are often relatively abrupt, spanning ∼100s km s^{-1}. These distinctive features would be hard to reconcile with absorption by individual clouds, but are consistent with the line of sight to a BAL quasar intersecting an outflow that is not entirely radial, e.g. an outflow which initially emerges perpendicular to the accretion disc and is then accelerated radially (Murray et al. 1995; Elvis 2000). N V BALs often absorb part of the Lyα emission line, so the BAL

★E-mail: crb@ing.iac.es

region must typically lie outside at least some of the broad emission-line region (BLR), i.e. >0.1 pc from the quasar nucleus. BALs are generally saturated (optical depth ∼ few) but non-black, implying partial covering of the nuclear regions (or infilling of the absorption troughs by scattered light). This means that column densities cannot be measured directly from apparent absorption depths (in the past this has led to incorrect inference of super-solar metallicities).

Formally, a BAL quasar is one with BALnicity index (BI, Weymann et al. 1991) greater than zero. BI is defined as the equivalent width of the C IV absorption, integrated over any contiguous region of the spectrum 3000–25 000 km s^{-1} blueward of the quasar velocity, spanning at least 2000 km s^{-1}, with continuum intensity <0.9 that of the assumed unabsorbed continuum. Shallower BAL-like features are seen in a larger fraction of quasars (Reichard et al. 2004), suggesting that many quasars have similar outflows. Absorbers similar to quasar BALs are seen in Seyfert 1 galaxies, albeit with lower outflow velocities, typically < few hundred km s^{-1} (see contributions in Crenshaw, Kraemer & George 2002).

The most prominent BALs are due to high-ionization species, particularly Li-like ions with one electron in the outer orbit: C IV 1549 Å, Si IV 1400 Å, N V 1240 Å. Quasars with absorption spectra dominated by these ions are known as high-ionization BALs (HiBALs). ∼15 per cent of BAL quasars also show absorption by lower-ionization species, such as Mg II 2798 Å and Al III 1858 Å, and are known as LoBALs. FeLoBALs are a small subset of the LoBALs showing absorption by Fe II and Fe III.

With few exceptions, no changes have been observed in the velocity structure of BALs on time-scales ∼10 yr. The intensity of the absorption does vary, probably due to changes in covering factor, which suggests that the absorbers are intrinsic to the quasar.

BAL quasars are typically weak in soft X-rays, probably because the X-ray emission is absorbed. The relationship between UV and X-ray absorbers was discussed by Blustin et al. (2005).

Several useful catalogues of BAL quasars exist. Korista et al. (1993) presented a sample of 72 C IV BALs. Becker et al. (2000, 2001) found 43 BALs in 3300 deg^2 of the FIRST Bright Quasar Survey ($S_{1.4\,GHz} > 1$ mJy). Large samples of quasars are now becoming available from the Sloan Digital Sky Survey (SDSS, York et al. 2000). Reichard et al. (2003a) found 224 BAL quasars in the SDSS Early Data Release quasar catalogue. This sample includes the 116 BALs found by Tolea, Krolik & Tsvetanov (2002), and it overlaps with that of Menou et al. (2001), who sought identifications of SDSS quasars with FIRST sources in 290 deg^2 (14 radio BALs). A catalogue of 23 unusual BALs found in SDSS (mainly LoBALs) was presented by Hall et al. (2002).

Hypotheses concerning the nature of BAL quasars differ mainly in the emphasis placed on the role of orientation. On the one hand, BALs may be present in all quasars but are intercepted by only ∼10–20 per cent of the lines of sight to the quasar, e.g. lines of sight skimming the edge of the accretion disc or torus (Weymann et al. 1991; Elvis 2000). Alternatively, BALs may arise in a physically distinct population of quasars, e.g. newborn quasars shedding their cocoons of gas and dust, or quasars with unusually massive black holes or with unusually high accretion rates (Briggs, Turnshek & Wolfe 1984; Boroson & Meyers 1992). Amongst optically selected quasars, evidence has accumulated to favour the orientation hypothesis. For example, in most respects, apart from the BAL itself, BAL quasars appear similar to normal quasars (Weymann et al. 1991). The small differences from non-BAL quasars, e.g. slightly redder continua (Reichard et al. 2003b) and higher polarization, could also be a consequence of a preferred viewing angle. The submillimetre properties of BALs are similar to those of non-BALs (Lewis, Chapman & Kuncic 2003; Willott, Rawlings & Grimes 2003), implying similar dust properties. This is consistent with the orientation hypothesis, but is difficult to reconcile with BAL quasars being an evolutionary stage associated with a large dust mass.

Until recently, very few radio-loud BAL quasars were known. This changed with the advent of the FIRST Bright Quasar Survey (FBQS, Becker et al. 2001), but few BALs are known with $\log R^* > 2$ (radio-loudness $R^* = S_{5\,GHz}/S_{2500\,Å}$, Stocke et al. 1992). Becker et al. (2001) estimated that BALs are four times less common amongst quasars with $\log R^* > 2$ than amongst quasars with $\log R^* < 1$. Hewett & Foltz (2003) note that optically bright BAL quasars are half as likely as non-BALs to have $S_{1.4\,GHz} > 1$ mJy. The dependence of the BAL fraction on R^* may reflect the higher ratio of X-ray to UV luminosity in radio-louder objects, which could overionize the gas, reducing the velocity to which line-driven winds can be accelerated (Murray et al. 1995). Becker et al. (2000) found that radio-selected BAL quasars have a range of spectral indices, which suggests a wide range of orientations, contrary to the favoured interpretation for optically selected quasars. Radio-loud BALs tend to be compact in the radio, similar to GHz-peaked spectrum (GPS) or compact steep-spectrum (CSS) sources, and GPS/CSS sources are thought to be the young counterparts of powerful large-scale radio sources (O'Dea 1998). This supports the alternative hypothesis that BALs represent an early phase in the life of quasars (Gregg et al. 2000).

In Boroson's (2002) scheme for the classification of active galactic nuclei (AGN), based on a principal-component analysis of AGN properties, the different observed types correspond to different combinations of $L/L_{Eddington}$ (luminosity as a fraction of Eddington luminosity) and dM/dt (the accretion rate). BAL quasars occupy one corner of this space, with $L/L_{Eddington} \sim 1$, similar to narrow-line Sy1 galaxies, but with a much higher accretion rate. The BAL quasar accretion rates are similar to those of radio-loud quasars, but with larger $L/L_{Eddington}$ (and lower-mass black holes). In Boroson's scheme, the rare radio-loud BAL quasars may be objects with extremely high accretion rates.

Lamy & Hutsemekers (2004) carried out a principal-component analysis of 139 BAL quasars with good-quality spectra and/or polarization measurements. They found that most of the variation is contained in two principal components. The first is dominated by a correlation between BI and the strength of the Fe II emission, and may be driven by the accretion rate. The second is due to the fact that BALs with PCyg profiles (i.e. absorption just blueward of the emission line) are more polarized than those with detached BALs. Detachment is thought to correlate with orientation, with the more detached BALs being seen if the angle of the line of sight to the disc is larger.

Hewett & Foltz (2003) found no evidence that the fraction of quasars with BALs varies with redshift for $z < 3$. However, at higher redshift, the fraction may rise. Maiolino et al. (2004) recently found that of eight $z > 4.9$ quasars observed, four showed strong BALs, with two of these having unusually high BALnicity index, and two being LoBALs (which are rare at low redshift). These results suggest that BALs are more common at high redshift, perhaps because of a higher accretion rate, which might affect the solid angle subtended at the quasar by the BAL flow, and thus the fraction of quasars observed to have BALs.

In short, the role of orientation in BALs is still not clear, and it is likely that detailed measurements of physical conditions within the outflows are required to make further progress. Studies of BAL outflows are also important: (1) for understanding accretion in AGN, where the inflow (fuelling) and outflow rates may be related through the need to shed angular momentum; (2) as probes of chemical enrichment in the central regions of AGN; (3) because the outflowing gas may contribute significantly to the metallicity of the IGM; (4) because the outflows may affect the subsequent evolution of the host galaxy (Silk & Rees 1998; Fabian 1999); and (5) because the physics of the outflowing gas is not understood. No self-consistent physical model yet exists for the acceleration of the gas, or, if the filling factor is small (many small clouds), for its confinement. Possible mechanisms for the acceleration include radiation pressure, pressure from cosmic rays or centrifugally driven magnetic disc winds (de Kool 1997). One possible signature of radiation pressure is absorption–absorption line-locking, and this has been observed in a few quasars (see Section 3.2.2).

1.1 NALs and mini-BALs

The blending of saturated features in BALs precludes measurement of the column densities, which are required to constrain the ionization balance, the distance of the absorber from the quasar and the physics involved in accelerating the outflows. However, some quasars show additional narrow absorption lines (NALs) with velocity widths small enough (FWHM $\gtrsim$ 300 km s^{-1}) that multiplets of individual ions can be resolved, allowing the covering factor and true optical depth to be determined independently (Arav et al. 1999). Some NALs are intrinsic to the quasar (associated absorption lines, AALs; see, e.g., Wise et al. 2004) and may be related to the BAL phenomenon. Intermediate in FWHM are the rarer (∼1 per cent of quasars, Hamann & Sabra 2004) mini-BALs, FWHM $\gtrsim$ 2000 km s^{-1}. The partial covering, variability and smooth absorption troughs indicate that mini-BALs are intrinsic outflows like those seen in BALs, but with the advantage that in some cases the covering factor and optical depth can be measured as a function of velocity. Mini-BALs are thus particularly useful for constraining physical conditions in the outflow.

Using mostly the *Hubble Space Telescope* (*HST*), Keck and VLT, high-resolution spectra of several intrinsic NAL and mini-BAL absorbers have been obtained, including those in quasars (full names abbreviated) 0011+0055 (Hutsemékers, Hall & Brinkmann 2004), 0300+0048 (Hall et al. 2003), 0449−13 (Barlow, Hamann & Sargent 1997), 08279+5255 (Srianand & Petitjean 2000), 0946+301 (Arav et al. 2001), 1037−2703 (Srianand & Petitjean 2001), 1044+3656 (de Kool et al. 2001), 1230+0115 (Ganguly et al. 2003), 1303+308 (Foltz et al. 1987; Vilkovskij & Irwin 2001), 1415+3408 (Churchill et al. 1999), 1511+091 (Srianand et al. 2002), 1603+3002 (Arav et al. 1999), 1605−0112 (Gupta et al. 2003), 2233−606 (Petitjean & Srianand 1999), 2302+029 (Jannuzi et al. 1996), UM675 (Hamann et al. 1997), in six quasars studied by D'Odorico et al. (2004) and in the Sy1 galaxy NGC 5548 (Arav, Korista & de Kool 2002). The earlier of these papers established the intrinsic nature of the absorbers and showed the importance, when measuring column densities, of taking into account saturation and the limited covering factor. These analyses also implied that the absorbers lie close to the quasar nucleus (although there are few actual measurements of distance) and might in some cases be identified with the X-ray warm absorbers.

Some of the quasars (0449−13, 0946+301, 1037−2703, 1303+308) show changes with time of covering factor. Only 1303+308 has shown any change in *velocity* (55 km s^{-1} increase in velocity over five rest-frame years). In some (0011+0055, 08279+5255, 2233−606), the covering factor varies with ion, perhaps because of inhomogeneous coverage (Hamann & Sabra 2004). In 1603+3002 the absorption covers the continuum, but not the broad-line region. 1415+3408 is unusual in that the covering factor in N V is close to unity, suggesting an unusual viewing angle. Several of these objects (see Section 3.2.2) show evidence of line-locking between individual velocity components.

In summary, intrinsic NALs and mini-BALs are excellent probes of the abundances and physical conditions in outflows close to the nuclei of quasars, with each object providing a fresh perspective.

1.2 Radio BAL quasar 1624+3758

Here we present a HiBAL quasar with unusual optical and radio properties. Quasar 1624+3758 (POSS $E = 18.1$, $O - E = 2.5$) was identified during a search for high-redshift quasars at the positions of FIRST radio sources, using the Isaac Newton Telescope (Benn et al. 2002; Holt et al. 2004). The radio source, $S_{1.4\,\mathrm{GHz}} = 56$ mJy, is at RA 16$^{\mathrm{h}}$ 24$^{\mathrm{m}}$ 53$^{\mathrm{s}}$.47, Dec. 37° 58′ 6″.7 (J2000), 0$^{\mathrm{s}}$.02E, 0″.0N of the POSS-I/APM (Automated Plate Measuring Machine, Cambridge) optical position. 1624+3758 is the most radio-luminous BAL quasar known (Fig. 1), $P_{1.4\,\mathrm{GHz}} = 4.3 \times 10^{27}$ W Hz^{-1}.

It is also highly luminous at optical wavelengths. The E mag implies M_{AB}(1450-Å) ≈ −27.6, $L_{1450\,\mathrm{Å}} \sim 5 \times 10^{24}$ W Hz^{-1} and $\nu L_\nu \sim 10^{47}$ erg^{-1}, corresponding to a total luminosity of $\sim 10^{47.6}$ erg^{-1}, using the bolometric correction of Warner, Hamann & Dietrich (2004).

1624+3758 is detected in the 2MASS survey (Cutri et al. 2003), with $J = 16.9$, $H = 16.3$, $K = 15.6$. No X-ray detection is recorded in the NED/IPAC extragalactic data base (NED).

The radio loudness of the quasar (defined above), calculated from the radio spectrum reported in Section 2.2, and the 2MASS J magnitude (rest-frame ≈2800 Å), is $R^* = 260$ (assuming no extinction in the UV). This meets the conventional definition of radio-loud, $\log R^* > 1$. Few BAL quasars are known with $\log R^* > 2$.

In this paper, we report high-resolution ($R = 10\,000$) optical spectroscopy of the quasar and radio observations. In Section 2, we present the optical and radio observations. The emission and absorption features are analysed in Section 3. In Section 4 we

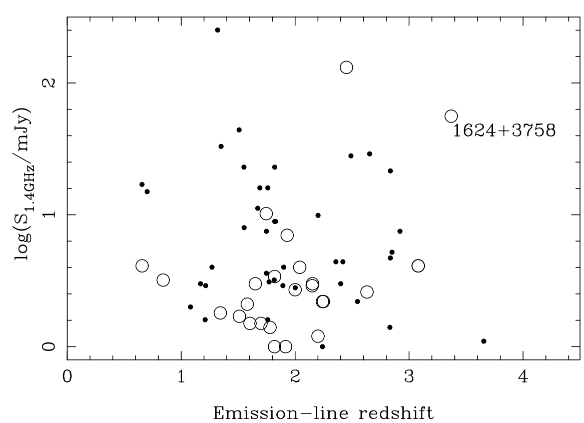

Figure 1. Distribution of known radio BAL (BI > 0) quasars in emission-line redshift and 1.4-GHz flux density (from the FIRST survey). Circles indicate BALnicity index BI > 2000 km s^{-1}. Dots indicate 0 < BI < 2000 km s^{-1}. The following samples are plotted: NVSS, Brotherton et al. (1998, five quasars); FBQS, Becker et al. (2000, 2001, 33 quasars); FIRST/SDSS, Menou et al. (2001, 11 quasars); SDSS, Reichard et al. (2003a, 15 quasars); Brotherton et al. (2002, two FRII BAL quasars, $S_{1.4\,\mathrm{GHz}} > 100$ mJy); and quasar 1624+3758 (labelled) reported in this paper. 1624+3758 is the most radio-luminous BAL quasar identified to date. Only the two FRII (>200 kpc) BAL quasars, plotted near the top of the figure, have a similar total radio luminosity. Most of the remaining quasars are unresolved by the FIRST survey, FWHM < 5 arcsec.

Table 1. Log of observations.

Date of observation (1)	Airmass (2)	Seeing (arcsec) (3)	Dichroic used (4)	ISIS arm (5)	Grating (6)	CCD (7)	Wavel. range (Å) (8)	Exposure (s) (9)	Resolution (Å) (10)	σ_λ (Å) (11)
2003 June 18	1.02	0.9	5700 Å	Blue	R600B	EEV12	4200–5700	2×1800	2.3	0.15
2003 June 18	1.02	0.9	5700 Å	Red	R600R	MAR2	5700–7300	2×1800	1.8	0.04
2003 July 2	1.73	0.9	Clear	Red	R1200R	MAR2	6200–7000	3×1800	0.8	0.04

discuss the nature of the quasar. Our conclusions are summarized in Section 5.

For consistency with earlier papers, we use throughout a cosmology with $H_0 = 50$ km s^{-1} Mpc^{-1}, $q_0 = 0.5$ and $\Lambda = 0$. Wavelengths are corrected to vacuum, heliocentric.

2 OBSERVATIONS

2.1 Optical spectroscopy

Spectra of 1624+3758 were obtained with ISIS, the dual-arm spectrograph of the 4.2-m William Herschel Telescope (WHT) on La Palma, on 2003 June 18 (service observation) and on 2003 July 2. The June spectrum covers the wavelength ranges 4200–5700 and 5700–7300 Å, with resolutions of 2.3 and 1.8 Å, respectively. The July spectrum covers the range 6200–7000 Å, with a resolution of 0.8 Å. The observing details are summarized in Table 1. All observations were carried out at the parallactic angle, in photometric conditions and with the Moon below the horizon.

The data were reduced in the usual way, using standard packages in IRAF for the bias subtraction, flat-fielding, cosmic ray removal, wavelength calibration and intensity calibration. The rms errors in wavelength calibration, determined by comparing the measured and published (Osterbrock et al. 1996) wavelengths of night-sky emission lines, are given in column 11 of Table 1 (the value for the June 18 blue-arm observation is an upper limit, since only a few faint sky lines were detected). The spectral resolution (column 10) was measured from the widths of the sky lines.

Intercomparison of the standard-star spectra suggests that the accuracy of the intensity calibration is ~5 per cent.

A low-resolution spectrum of the quasar (FWHM ≈ 4 Å in the red) was obtained in 2003 by the Sloan Digital Sky Survey (SDSS data release 3, Abazajian et al. 2005). The SDSS apparent magnitudes are $u = 22.4$, $g = 19.1$, $r = 18.5$, $i = 18.2$ and $z = 18.0$.

2.2 Radio observations

We observed 1624+3758 with the 100-m Effelsberg radio telescope at 4.85 and 10.45 GHz on 2003 December 18 and 2004 January 17, respectively. The cross-scanning technique used is described by Vigotti et al. (1999) and references therein. 3C286 was used as a flux-density calibrator.

We also observed 1624+3758 with the Very Large Array (VLA) radio telescope in C configuration, at 8.5 GHz (exposure time of 20 min) and 22.5 GHz (exposure time of 40 min), on 2004 March 24. The nearby source 1613+342 was used as a phase calibrator. Initial images of the source contained sufficient flux density to permit local self-calibration to remove residual phase errors. 3C286 was used as a flux-density calibrator. The data were reduced with the IMAGR program in the AIPS package.

We also observed the quasar with the Westerbork Synthesis Radio Telescope (WSRT) for 3 h on 2004 July 1. The 2.2-GHz flux density was measured, but only a 3σ upper limit on the polarization could be obtained, due to a combination of radio interference and technical problems.

Our radio observations are summarized, with others from the literature, in Table 2, and the spectral energy distribution is shown in Fig. 2. The spectrum is steep at high radio frequencies, $\alpha = -0.9$ ($S_\nu \propto \nu^\alpha$).

At 22.5 GHz, the source is resolved by the VLA (size 0.4 ± 0.1 arcsec). This implies a projected linear size of ≈2.8 kpc, i.e. this is a compact steep spectrum (CSS) source, as are most radio BAL quasars (Becker et al. 2000). 1624+3758 is one of the most distant CSS sources known. The spectrum turns over at low frequency, probably due to synchrotron self-absorption. The rest-frame turnover frequency ≈2 GHz provides an independent estimate of size, ~0.1–1 kpc (using the relationship given by O'Dea 1998).

The steep radio spectral index implies that the source is lobe-dominated. The spectrum at frequencies higher than 1 GHz shows

Table 2. Radio observations of 1624+3758.

Telescope	Freq. (GHz)	Resolution (arcsec)	Flux density (mJy)	±	Polarization (per cent)	±	PA (deg)	±	Survey
VLA (B)	0.074	80	< 220						VLSS
WSRT	0.325	54	72	5.3					WENSS
VLA (D)	1.40	45	55.6	1.7	< 2.2				NVSS
VLA (B)	1.40	5	56.4	1.5					FIRST
WSRT	2.27	36	38.5	0.8	< 2.3				this paper
Effelsberg	4.85	120	23.3	1.1	1.7	0.7	−152	7	this paper
VLA (C)	8.46	2.4	15.0	0.09	6.5	0.3	−7	4	this paper
Effelsberg	10.45	270	10.5	0.8	11.0	3.0	19	5	this paper
VLA (C)	22.46	0.9	5.4	0.02	11.3	1.5	45	13	this paper

The flux densities are all on the scale of Baars et al. (1977). The surveys are: VLSS = VLA Low-frequency Sky Survey (Kassim et al. 2003); WENSS = Westerbork Northern Sky Survey (Rengelink et al. 1997); NVSS = NRAO VLA Sky Survey (Condon et al. 1998); FIRST = Faint Images of the Radio Sky at Twenty-cm (White et al. 1997). PA = position angle of polarization.

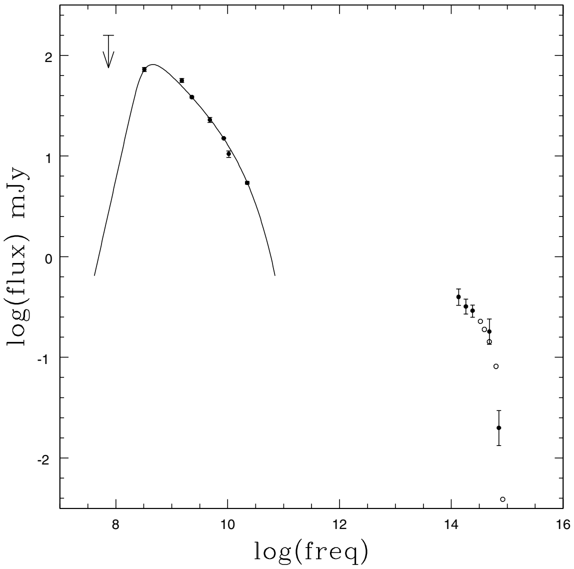

Figure 2. Spectral-energy distribution of BAL quasar 1624+3758. The radio flux-density measurements are summarized in Table 2. The higher-frequency measurements are from the 2MASS survey (*K*, *H* and *J* bands), from the APM catalogues of objects on POSS-I (*E* and *O* bands) and from SDSS (no error bars plotted). The radio spectrum turns over near 500 MHz, due to synchrotron self-absorption at lower frequencies. The solid curve is a fit by a synchrotron ageing model (Section 2.2).

significant curvature (it cannot be fitted with a simple power law), which we attribute to ageing of the population of relativistic electrons responsible for the synchrotron emission (Murgia et al. 1999). We fitted the observed spectrum with two popular ageing models: the continuous-injection (CI) model of Pacholzcyk (1970), which assumes continuous replenishment within each resolution element of particles and energy lost through synchrotron radiation; and the model of Jaffe & Perola (1973, JP), which predicts spectral ageing assuming no replenishment. Fitting the spectrum with these models yields the break frequency $\nu_{\rm br}$ at which the spectrum starts to turn down as a result of synchrotron losses. The particle ages are then given by

$$\tau = 1610 \frac{B^{1/2}}{B^2 + B_{\rm CMB}^2} \frac{1}{\sqrt{\nu_{\rm br}(1+z)}} \text{ Myr}$$

(Murgia et al. 1999), where B is the source magnetic field in μG, $B_{\rm CMB}$ is the magnetic field strength corresponding to the cosmic microwave background [CMB, $B_{\rm CMB} = 3.25(1+z)^2$ μG] and $\nu_{\rm br}$ is in GHz. The JP model fits the data better than the CI model, as is often the case for relic sources in which activity has ceased. The fitted break frequencies $\nu_{\rm br}$ are $7.6^{+1.7}_{-1.3}$ GHz for the CI model and $38.0^{+4.8}_{-3.8}$ GHz for the JP model. If equipartition of energy between the magnetic field B and relativistic particles is assumed, then (following Miley 1980) $B = 740$ μG. Even using the lower estimated $\nu_{\rm br}$ (from the CI model), this yields a maximum particle age of <15 000 yr, which is typical of synchrotron ages found for lobe-dominated CSS sources (e.g. Murgia et al. 1999).

The radio emission in 1624+3758 is therefore of recent origin compared with the typical age of an evolved radio source, $\sim 10^7$ yr.

The position angle (PA) of the polarization was measured at each of 4.85, 8.46, 10.45 and 22.46 GHz (the source is depolarized at frequencies $\leqslant$2.2 GHz). From the variation with wavelength (Fig. 3), we determine the rotation measure, RM (ΔPA = RM $\Delta\lambda^2$) to be 960 ± 30 rad m^{-2}, which in the rest frame of the source is a factor of $(1+z)^2$ higher, i.e. 18 350 ± 570 rad m^{-2}. This is the second-highest RM known, after that of quasar OQ172 (Kato et al. 1987; O'Dea 1998), RM = 22 400 rad m^{-2}. OQ172 is not a BAL quasar. In a recently published compilation of parsec-scale RM in AGN, Zavala & Taylor (2004) found a median RM of 2000 rad m^{-2} and no AGN with RM > 10 000 rad m^{-2}.

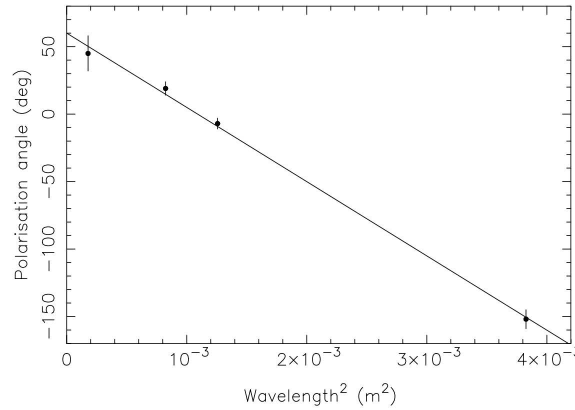

Figure 3. Derivation of the rotation measure RM from the radio observations. The straight line has slope RM = −960 rad m^{-2}. This is the second highest RM known amongst AGN.

The rotation measure is proportional to $n_{\rm e} B_{||} l$, where $n_{\rm e}$ is the electron density, $B_{||}$ is the magnetic field strength along the line of sight and l is the effective path-length along the line of sight, so an unusually high value of RM implies a high value of at least one of these parameters.

3 RESULTS OF OPTICAL SPECTROSCOPY

Fig. 4 shows the ISIS spectrum of 1624+3758 obtained 2003 June 18. Figs 5 and 6 show the spectrum at higher dispersion. Emission and absorption features are listed in Tables 3 and 4, respectively. Derived column densities are listed in Table 5.

We discuss the emission lines in Section 3.1. The absorption features include: a mini-BAL (defined as a BAL-like feature spanning <2000 km s^{-1}, Section 3.2, Figs 8–10); a possible associated (i.e. $v > -3000$ km s^{-1}) absorber with large H I column density (Section 3.3); a BAL (Section 3.4); and nine NALs (two probably associated and seven intervening, Section 3.5).

The spectral index of the continuum between observed wavelengths 7000 and 9000 Å (rest-frame 1600–2060 Å) is $\alpha_\lambda = -0.7$ ($f_\lambda \propto \lambda_\lambda^\alpha$), $\alpha_\nu = -1.3$, slightly redder than most HiBAL quasars (Reichard et al. 2003b), similar to the median for LoBAL quasars, and suggesting dust reddening $E(B-V) \approx 0.07$ mag relative to non-BAL quasars, assuming extinction by Small Magellanic Cloud-type dust (Pei 1992). (The much redder broad-band colour of the quasar, $O - E = 2.5$, is due to the drop in the continuum across Lyα.)

3.1 Emission lines and quasar redshift

The centroid wavelengths of the Lyα, N V, O I, C II, Si IV and C IV emission lines are given in column 4 of Table 3. Lyβ 1026 Å, O VI 1035 Å and He II 1640 Å are not detected in emission.

The high-ionization lines N V and C IV are blueshifted a few 100 km s^{-1} with respect to the low-ionization lines, as in most quasars (Gaskell 1982; Tytler & Fan 1992; Richards et al. 2002b). To obtain a system redshift $z_{\rm sys}$ (usually closer to that of the low-ionization

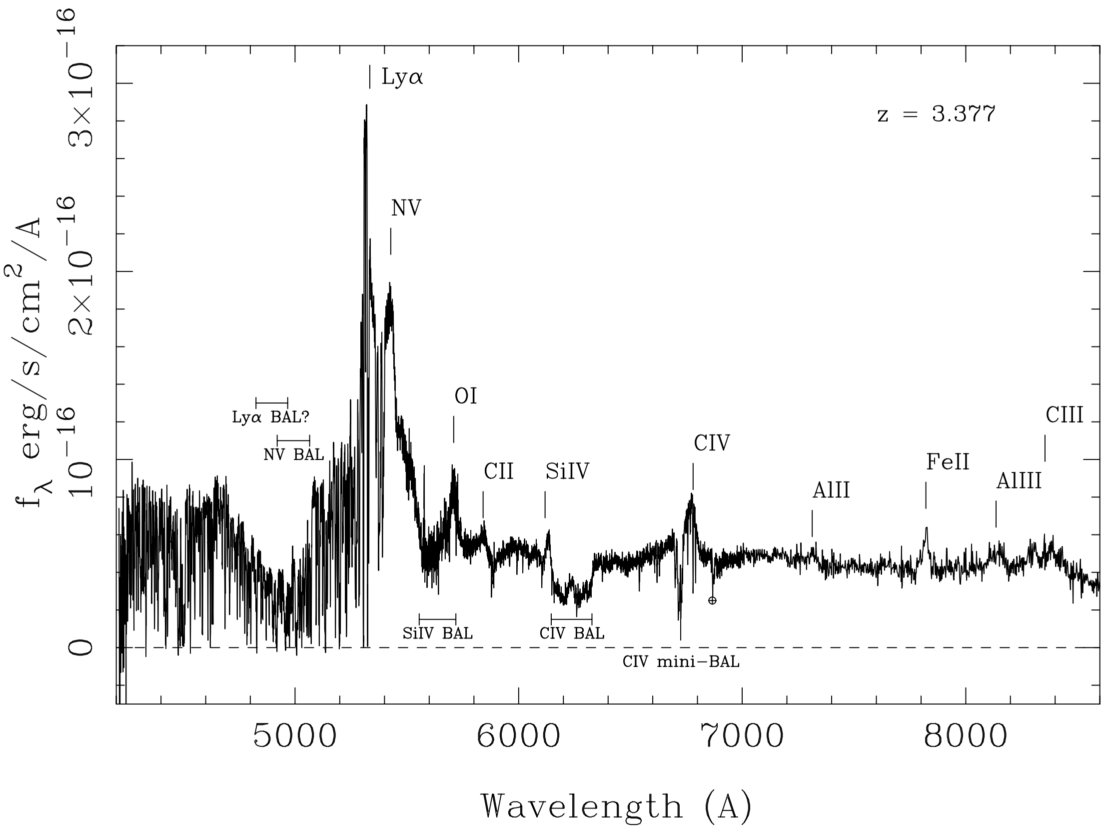

Figure 4. Spectrum of BAL quasar 1624+3758 taken with the WHT ISIS spectrograph 2003 June 18. The blue- and red-arm spectra are joined at 5730 Å. The spectrum redward of 7000 Å is from the lower-resolution observation of this quasar in SDSS data release 3. The ticks above the emission lines indicate the wavelengths expected for redshift 3.377, assuming the $\lambda_{\rm lab}$ wavelengths given in Table 3. Horizontal bars indicates the C IV BAL outflow, velocity −20 700 to −29 300 km s^{-1} and the expected wavelengths of absorption by H I, N V and Si IV ions with a similar range of velocity. The mini-BAL just blueward of the C IV emission line ranges in velocity from −2200 to −3400 km s^{-1}. It is also detected in N V (≈5370 Å, see Fig. 5) and in O VI (≈4490 Å, see Fig. 5). The feature at 6867 Å is uncorrected telluric absorption (*B* band).

lines than that of the high-ionization lines), we use the modified emission-line wavelengths $\lambda_{\rm sr}$ tabulated by Tytler & Fan. These take into account the velocity shifts and approximate $\lambda_{\rm observed}/(1 + z_{\rm sys})$. Tytler & Fan do not give a modified wavelength for C II, but this is a low-ionization line, so we assume zero velocity shift relative to the quasar, i.e. $\lambda_{\rm sr} = \lambda_{\rm lab} = 1334.53$ Å. The observed emission-line wavelengths are consistent with a quasar redshift $z = 3.377 \pm 0.003$. Column 8 of Table 3 gives the velocity of each line relative to this redshift. Column 9 gives the velocity relative to the mean for that line found by Tytler & Fan (typical dispersions of ∼200 km s^{-1}). The Si IV line in 1624+3758 is significantly redshifted relative to the other lines, but is blended with an O IV emission line, which might be strong in this quasar, given that the O I 1304-Å line is unusually strong.

The C IV emission line is blueshifted relative to the quasar by 320 km s^{-1}, similar to the shifts found by Tytler & Fan for other quasars. The line is markedly asymmetric at its base (and the N V emission line has similar form, Fig. 7), consistent with the suggestion by Richards et al. (2002b) that the apparent blueshift of C IV lines is due to the red wings of the lines being suppressed, perhaps in part due to dust obscuration of emission from outflows on the far side of the nucleus (see their fig. 11).

The rest-frame FWHM of the C IV line (inferred from the blue half of the line) is 2300 km s^{-1}. In conjunction with the observed total luminosity (Section 1.2), this implies (Kaspi et al. 2000; Warner et al. 2004) a black hole mass $M_{\rm BH} \sim 10^9\,{\rm M}_{\odot}$. This is similar to masses determined by Lacy et al. (2001) for quasars of similar radio luminosity. It implies a high Eddington ratio $L/L_{\rm Eddington} \approx 2.0$, near the maximum found for quasars by Warner et al. (2004).

The O I line is prominent, equivalent width, EW ∼ 4 Å, compared with 1.7 Å in the SDSS composite quasar spectrum of Vanden Berk et al. (2001) and ∼1.8 and 5.0 Å in the composite HiBAL and LoBAL spectra of Reichard et al. (2003a). Bright O I emission is more common amongst those Reichard et al. BAL quasars with FIRST radio detections, $S_{1.4\,\rm GHz} > 1$ mJy (six out of nine, $z < 3$) than amongst those without radio detection (seven out of 31, $z < 3$).

The prominent emission line at an observed wavelength of 7822.7 Å, EW = 3.8 Å, corresponding to a rest-frame wavelength of 1787.2 Å (Fig. 4), is detected in the SDSS composite spectrum and is probably the Fe II UV191 triplet at 1785/1787/1788 Å. In 1624+3758, this line is unusually strong, with rest-frame EW = 3.8 Å, compared with 0.3 Å in the SDSS composite spectrum, and ∼0.4 and 1.7 Å in the composite HiBAL and LoBAL spectra of Reichard et al. (2003a). The Fe II/C IV EW ratio is also high (∼0.5) compared with 0.01 for the SDSS composite, and ∼0.02 and 0.1 for the Reichard et al. HiBAL and LoBAL composites.

Fe II 1787 Å is detected in the SDSS spectra of only one out of 40 randomly selected non-radio BALs (half $z < 3$, half $z > 3$) from the catalogue of Reichard et al. (2003a), and in only one out of 20 non-radio LoBAL quasars from that catalogue. However, it is detected in the spectra of four out of the 14 BALs from that catalogue which have radio counterparts in the FIRST catalogue, $S_{1.4\,\rm GHz} > 1$ mJy.

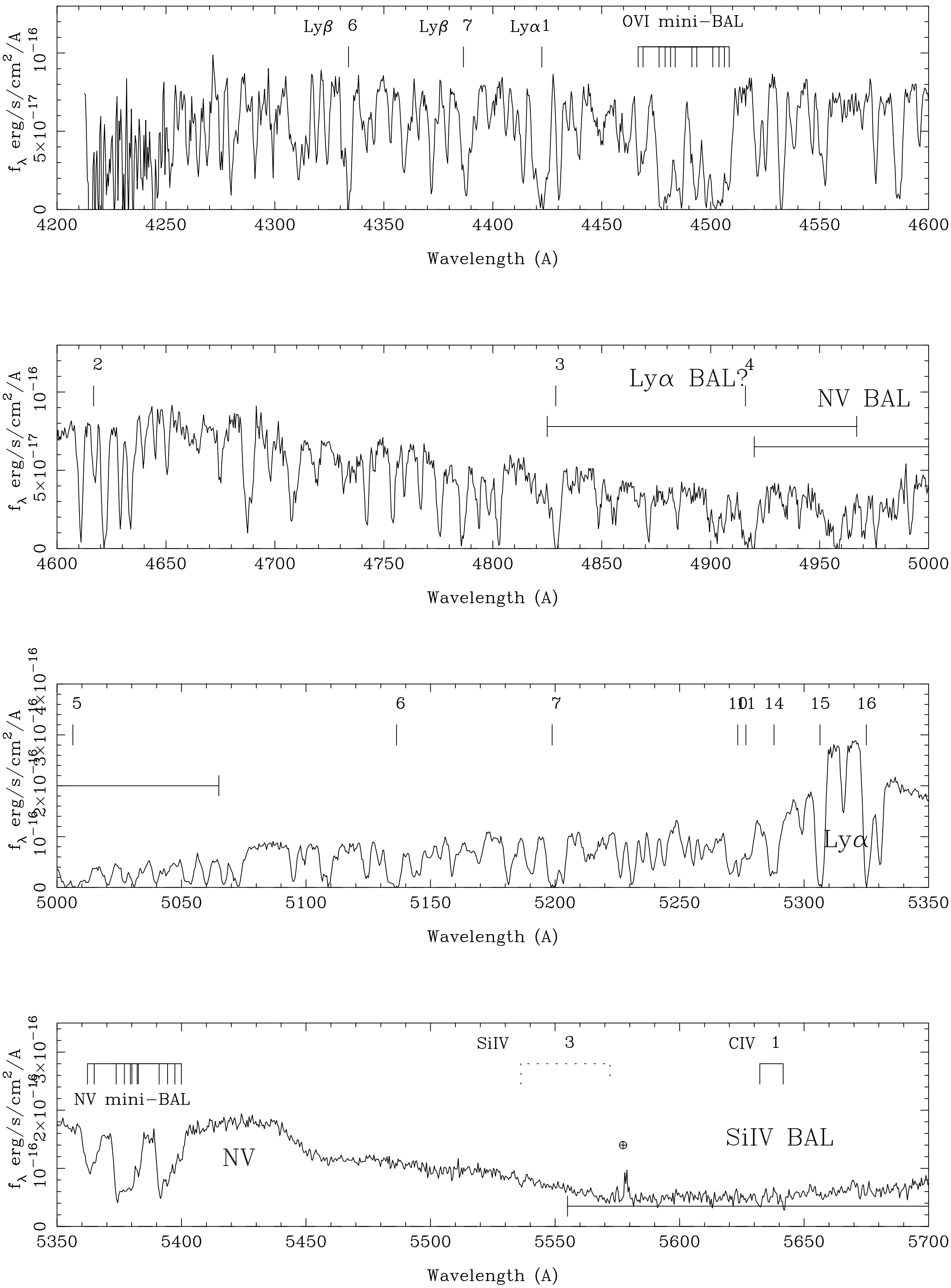

Figure 5. WHT ISIS blue-arm spectrum of BAL quasar 1624+3758, taken on 2003 June 18, plotted at higher dispersion than in Fig. 4. The ticks indicate detected absorption features (Lyα unless otherwise labelled) corresponding to the redshifts listed in Table 4 (laboratory wavelengths given in Table 3). The quasar Lyα and N V emission lines are also labelled (large font). The long horizontal bars indicate the expected range of wavelengths of absorption by Lyα, N V and Si IV ions at the same velocity as the C IV BAL. A feature due to poor subtraction of the 5577-Å airglow is marked.

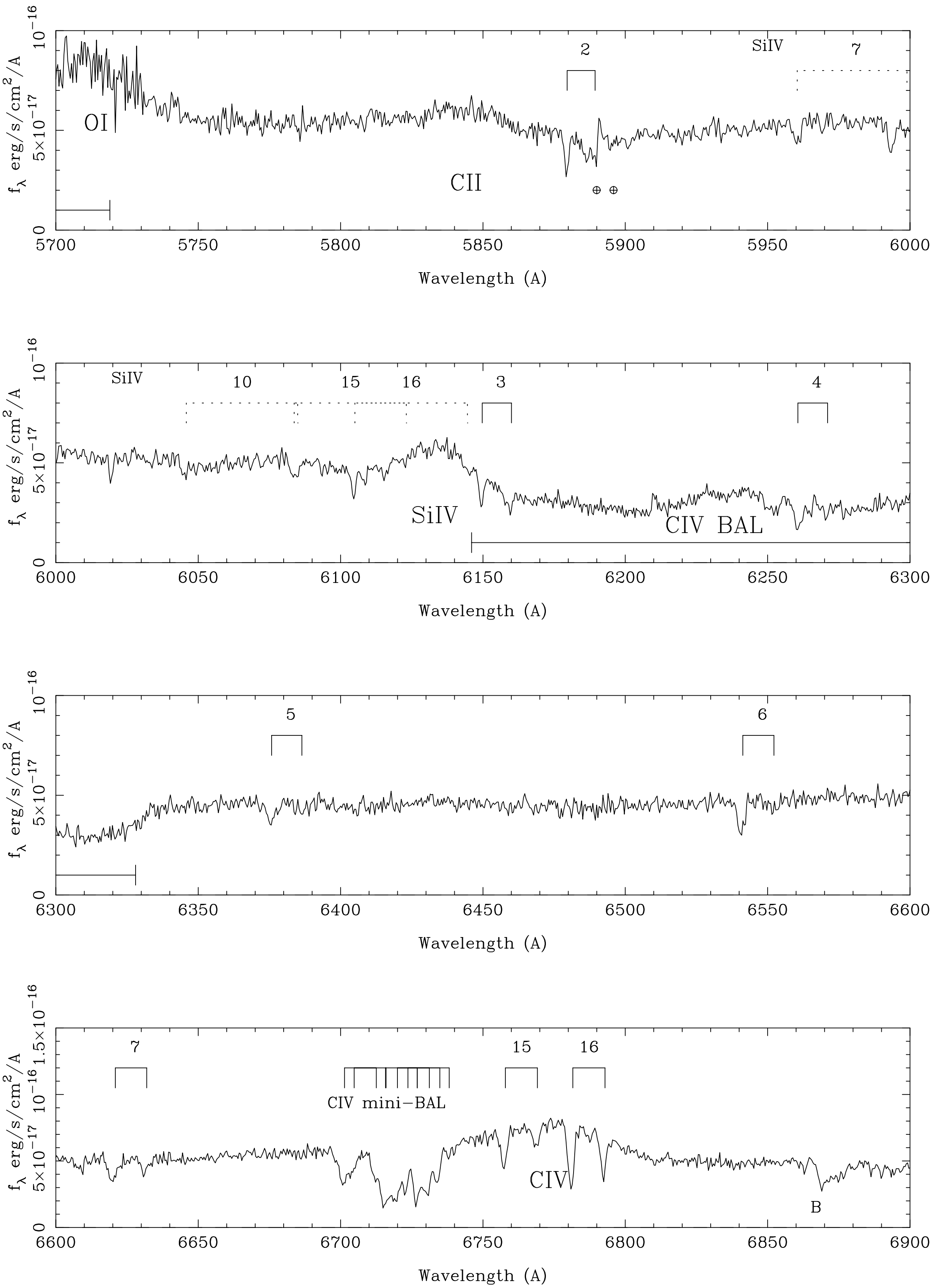

Figure 6. WHT ISIS red-arm spectrum of quasar 1624+3758, taken on 2003 June 18, plotted at higher dispersion than in Fig. 4, as in Fig. 5. The O I, C II, Si IV and C IV emission lines are labelled. The ticks indicate C IV (solid lines) and Si IV (dotted lines) absorption doublets. The red component of the C IV doublet of absorber 2 may be confused by the blue component of the NaD sky-line doublet (indicated). 'B' marks the uncorrected atmospheric absorption feature at 6867 Å. The weak absorption at 5992 and 6018 Å (also seen in the SDSS spectrum) could be additional C IV absorbers, but in neither case is the second component of the doublet detected.

Table 3. Emission lines in the spectrum of 1624+3758

Line	λ_{lab} (Å)	λ_{sr} (Å)	$\lambda_{observed}$ (Å)	± (Å)	z_{qso}	±	v (km s^{-1})	v_{sr} (km s^{-1})	Notes
(1)	(2)	(3)	(4)	(5)	(6)	(7)	(8)	(9)	(10)
Lyα	1215.67	1214.97	5314.7	3	3.3743	0.0025	−350	−180	
N V	1238.82 / 1242.80	1239.16	5420.2	2	3.3741	0.0016	−430	−200	
O I	1302/4/6 triplet	1304.24	5713.6	5	3.3808	0.0038	210	260	Confused by S IV BAL?
C II	1334.53	1334.53	5844.7	3	3.3796	0.0022	150	180	
Si IV	1393.75 / 1402.77	1398.62	6131.6	3	3.3840	0.0021	630	480	Si IV/O IV*
C IV	1548.20 / 1550.78	1547.46	6771.2	3	3.3757	0.0019	−320	−90	

The columns give: (1) line; (2) laboratory vacuum wavelength; (3) representative wavelength tabulated by Tytler & Fan (1992) for obtaining z_{qso}; (4, 5) observed wavelength and error; (6, 7) implied quasar redshift and error; (8) velocity of line relative to the assumed quasar $z = 3.377$ (negative velocity = blueshift); (9) velocity of line relative to mean from Tytler & Fan; (10) notes.
The weaker emission lines detected in the SDSS spectrum redward of 7000 Å have not been used for estimating the redshift.
For convenience, we note here the laboratory vacuum wavelengths of the other lines mentioned in this paper: Lyβ 1025.72; O VI 1031.93, 1037.62; Al II 1670.79; Fe II 1785/7/8; Al III 1854.72, 1862.79; C III] 1908.73 Å.
*The doublet wavelengths are for Si IV. The Si IV emission is usually blended with an O IV multiplet at 1402 Å.

Table 4. Absorption lines detected in the spectrum of 1624+3758.

Ref. no	z_{abs}	Velocity (km s^{-1})	Lines detected	dλ (Å)	R (Å)	FWHM$_b$ (Å)	EW_b (Å)	FWHM$_r$ (Å)	EW_r (Å)	Notes
(1)	(2)	(3)	(4)	(5)	(6)	(7)	(8)	(9)	(10)	(11)
1	2.6379	−54 863	Lyα C IV	−0.1	2.3	2.1	0.24	1.7	0.19	
2	2.7977	−42 307	Lyα C IV		1.8	1.6	0.16		∼0.15	Second line of C IV doublet obscured by NaD sky line
3	2.9722	−29 022	Lyα Si IV C IV	−0.1	1.8	1.6	0.14	∼2.5	∼0.21	
4	3.0438	−23 704	Lyα C IV	0.2	1.8	3.1	0.30	∼1.6	0.11	Resolved
5	3.1182	−18 262	Lyα C IV	∼0.5	1.8	2.2	0.12	2.0	0.05	
6	3.2251	−10 592	Lyβ Lyα C IV	∼0.6	0.8	1.4	0.11	∼2.6	0.17	Resolved
7	3.2765	−6 967	Lyβ Lyα Si IV C IV	∼0.0	0.8	2.5	0.34	4.1	0.24	Resolved
8	3.3283	−3 356	O VI N V C IV	∼0.1	0.8					
9	3.3307	−3 190	C IV		0.8					
10	3.3378	−2 699	O VI Lyα N V Si IV C IV	0.0	0.8					
11	3.3405	−2 512	O VI Lyα N V C IV	−0.3	0.8					
12	3.3429	−2 346	N V C IV	−0.1	0.8					
13	3.3450	−2 201	N V		0.8					
14	3.3498	−1870	Lyβ Lyα		0.8					Possible LLS
15	3.3650	−824	Lyβ Lyα Si IV C IV	0.6	0.8	2.1	0.22	1.4	0.10	Strong C IV, resolved
16	3.3803	206	Lyβ Lyα Si IV C IV	0.3	0.8	1.8	0.32	2.0	0.26	Strong C IV, resolved

The columns give: (1) absorber reference number; (2) redshift measured from the blue component of the C IV doublet (or N V for absorber 13, Lyα for absorber 14), rms error 0.0001; (3) absorber velocity relative to the assumed quasar redshift 3.377 (Section 3.1), calculated using $v/c = (R^2 - 1)/(R^2 + 1)$, $R = (1 + z_{em})/(1 + z_{abs})$; (4) ions detected in absorption; (5) observed − expected (≈11 Å) separation of C IV doublet (observed-frame); (6) resolution of the spectrum from which the FWHM and equivalent widths were measured; (7–10) observed-frame FWHM and rest-frame equivalent widths of blue and red components of C IV absorption line; (11) notes. All of the C IV absorbers with $z > 3.0$ are detected in both the June 18 and July 2 ISIS red-arm spectra, except that absorber 9 is detected only in the (higher-resolution) July 2 spectrum.
Absorbers 1–7 are probably intervening absorbers (i.e. not associated with the quasar). Absorbers 8–13 are components of the mini-BAL. Absorbers 14–16 are probably intrinsic, 'associated', absorbers.

The Fe II/C IV ratio in 1624+3758 is higher than in any of these objects.

The two relatively narrow emission lines at 1896.2 and 1915.1 Å, superimposed on the broad (and weak) C III] emission line (Fig. 4) are probably the two bluer components of the Fe III UV34 triplet at 1895.5/1914.1/1926.3 Å.

These Fe II and Fe III emission lines have also been observed in BAL quasar H0335−336 (Hartig & Baldwin 1986) and in quasar 2226−3905 (Graham, Clowes & Campusano 1996). Graham et al. note that the Fe II UV191 line is probably produced by dielectric recombination from Fe^{2+}, i.e. it is not surprising to observe it in association with Fe III lines.

3.2 Mini-BAL absorber, 3.3283 < z < 3.3450

The complex C IV absorption feature at outflow velocity −2200 to −3400 km s^{-1} (Fig. 8) is a 'mini-BAL', since the total velocity range is <2000 km s^{-1}.

Five individual velocity components can be identified, with the C IV doublet being well resolved in each case. The velocity

Table 5. Derived column densities of absorbers in 1624+3758.

Absorber (and ref. no) (1)	Velocity ($km\ s^{-1}$) (2)	log N (cm^{-2}) H I (3)	O VI (4)	N V (5)	Si IV (6)	C IV (7)	Cov fac (8)
BAL	−21 000 to −29 000					>16.0	0.3
Mini-BAL (12)	−2300 to −2450	>14	15.1	14.7	⩽13.2	14.7	0.6
LLS (14)	−1870	18.6	<13.6	<13.4	<12.5	<13.1	0.7
AAL (15)	−824	≳18.0			13.0	13.7	1.0
AAL (16)	206	≳18.0			13.0	13.9	1.0

For the BAL and mini-BAL, the column densities or limits were calculated using $N(v) = 3.77 \times 10^{14}\, \tau f^{-1} \lambda^{-1}\, \mathrm{d}v\ \mathrm{cm}^{-2}$ (Savage & Sembach 1991), where the oscillator strengths f are taken from Verner, Barthel & Tytler (1994), laboratory wavelengths λ are given in Table 3, and v is in km s^{-1}. The metal-line column densities for the LLS and AALs were calculated from the rest-frame equivalent widths, EW, using the alternative formulation: $N = 1.13 \times 10^{20}\ \mathrm{EW}\ f^{-1} \lambda^{-2}\ \mathrm{cm}^{-2}$ (Morton 2003). The N(H I) column density of the LLS (absorber 14) is from a Voigt-profile fit to the damping wings (Fig. 13). The N(H I) column density limits for the AALs are derived from the Lyα curve of growth. The covering factors C (column 8) are for C IV, except for the LLS, C measured from Lyα.

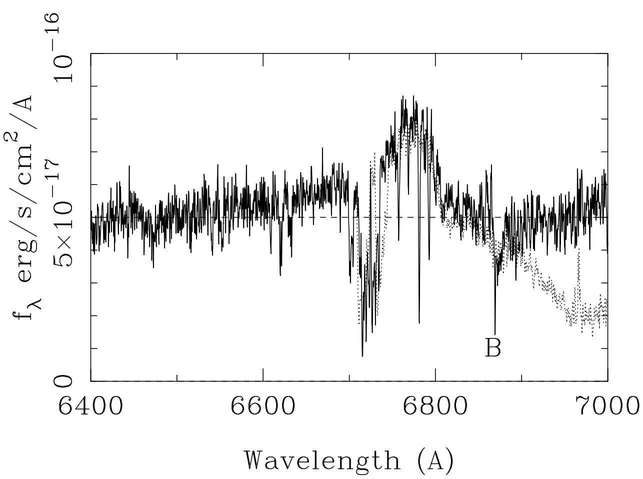

Figure 7. The C IV emission line (6771 Å) is asymmetric, with a broader wing to the blue than to the red. The dashed horizontal line shows the approximate level of the underlying continuum. The overplotted (dotted) curve shows the similar asymmetry in the core of the N V emission line.

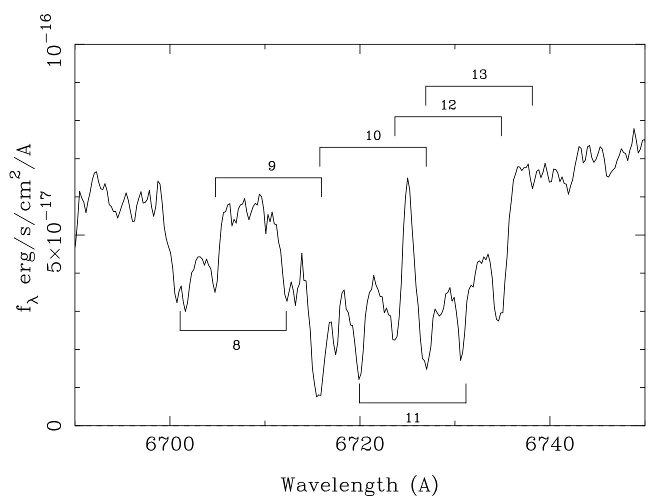

Figure 8. The spectrum of the C IV mini-BAL, taken with ISIS 2003 July 2 (instrumental resolution 0.8 Å, or 36 km s^{-1}). The ticks indicate the expected observed-frame wavelengths of the C IV doublet (1548.20, 1550.78 Å), for each of the redshifts identified in Section 3.2 (Table 4). The expected wavelengths for component 13 (detected in N V only, Fig. 9) are also indicated.

components are listed in Table 4. All are also detected in N V (Fig. 9), but with some blending of the components because of the lower spectral resolution. An additional absorber (13) is detected in N V. The mini-BAL is also detected in O VI (Fig. 10), but is confused by the Lyα forest. Absorber 10 is detected in Si IV (Fig. 6).

The mini-BAL is observationally unusual in exhibiting significant velocity structure, but without blending between the two components of the C IV doublet. This allows the covering factor and optical depth to be measured independently.

The variation of covering factor with velocity (below) and the large velocity spread (much greater than that expected for a galaxy halo) suggest that the mini-BAL is intrinsic to the quasar.

3.2.1 Local covering factor and optical depth

The observed depth of an absorption feature depends on the optical depth τ of the absorbing cloud and on the fraction C of the source which the cloud covers (or, more generally, on C as a function of τ). The similarity of the C IV and N V mini-BAL profiles (Figs 8 and 9) suggests that the form of the mini-BAL is dominated by variations in local covering factor C rather than by variations in optical depth. If the form of the mini-BAL were due to variation of optical depth, it is unlikely, given the different ionization potentials and abundances of C IV and N V, that this would result in similar C IV and N V absorption profiles.

Given observations with sufficient signal-to-noise ratio of two absorption lines of a particular ion for which the ratio of the optical depths is known, one can solve for both C and τ. For the C IV doublet, the ratio of the optical depths in the blue and red components is that of the oscillator strengths, $\tau(\mathrm{red}) = \tau(\mathrm{blue})/2$. Then the residual intensities in the red and blue components of the line, expressed as a fraction of the continuum intensity, are (Barlow & Sargent 1997; Arav et al. 1999):

$$I_\mathrm{r} = (1 - C) + C\mathrm{e}^{-\tau/2}$$

$$I_\mathrm{b} = (1 - C) + C\mathrm{e}^{-\tau},$$

where τ is the optical depth in the blue component of the doublet. These equations can be solved for C:

$$C = \left(I_\mathrm{r}^2 - 2I_\mathrm{r} + 1\right)/(I_\mathrm{b} - 2I_\mathrm{r} + 1)$$

(as long as $I_\mathrm{r} \geqslant I_\mathrm{b} \geqslant I_\mathrm{r}^2$) and for τ.

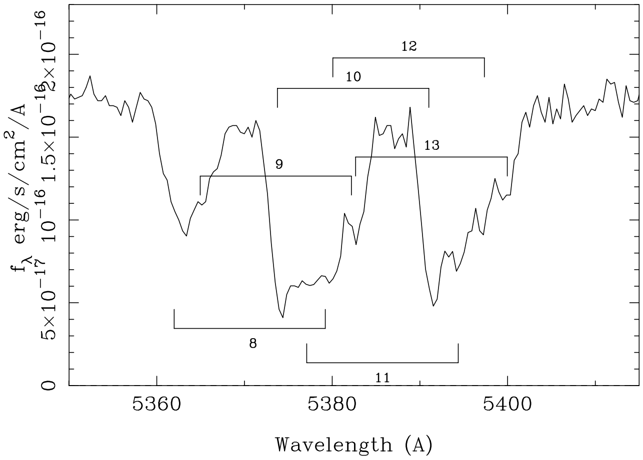

Figure 9. The mini-BAL in N V from the 2003 June 18 spectrum (the July spectrum does not include these wavelengths). The ticks indicate the expected observed-frame wavelengths of the N V doublet (1238.82, 1242.80 Å), for each of the redshifts in Fig. 8. Absorber 13 is detected only in N V. The spectral resolution is a factor of ≈3 poorer than that of Fig. 8.

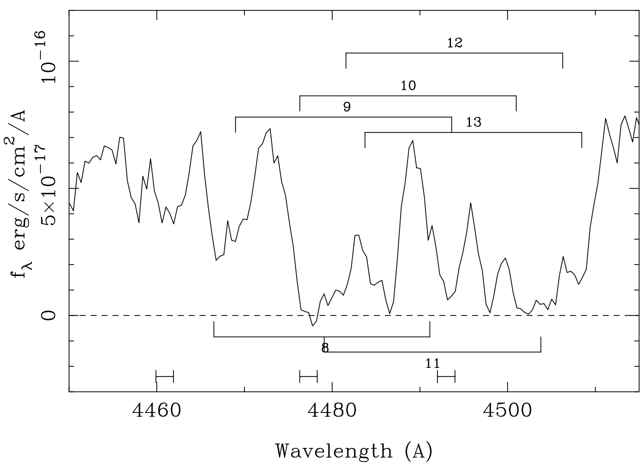

Figure 10. The mini-BAL in O VI from the 2003 June 18 spectrum. The ticks indicate the expected observed-frame wavelengths of the O VI (1031.93, 1037.62 Å) absorption, for each of the components shown in Figs 8 and 9. This region of the spectrum falls within the Lyα forest. It is also confused by Lyβ absorbers 14, 15 and 16 (expected wavelengths indicated by short bars at the bottom of the figure).

The derivation of C and τ from $I_{\rm b}$ and $I_{\rm r}$ is shown graphically in Fig. 11. Permitted combinations of $I_{\rm b}$ and $I_{\rm r}$ (i.e. satisfying the above inequalities) fall in the unshaded region of the figure. The figure highlights the need for a good signal-to-noise ratio in carrying out this type of analysis, with the errors on derived C and $e^{-\tau}$ being comparable to the errors on $I_{\rm b}$ and $I_{\rm r}$ over much of the allowed range. It also gives an overview of the effects of errors in $I_{\rm b}$ or $I_{\rm r}$ due to inadequate spectral resolution or to contamination of one of the two lines. For example, with inadequate resolution, a narrow saturated feature, with $C = 1$, $e^{-\tau} = 0$ and true $I_{\rm b} = 0$, $I_{\rm r} = 0$, may be observed as a broader unsaturated feature, with $I_{\rm b} > 0$, $I_{\rm r} > 0$, causing C to be underestimated and $e^{-\tau}$ to be overestimated. Fig. 11 also illustrates how C and τ are constrained by mere limits on $I_{\rm b}$ and $I_{\rm r}$. For example, if $I_{\rm b} < 0.2$, C must be >0.8.

The C IV mini-BAL shows similar velocity structure in each component of the doublet (Fig. 8), and the components are (just) unblended, with the intensity between them, near the observed wavelength of 6724 Å, being close to that of the continuum just blueward or redward of the mini-BAL. The derived values of C and τ for the C IV mini-BAL (absorbers 10–12) are shown as a function of velocity in Fig. 12(a). Note that the locus of measured $I_{\rm b}$ and $I_{\rm r}$ in Fig. 11 remains within the region of physically meaningful solutions $I_{\rm r} \geqslant I_{\rm b} \geqslant I_{\rm r}^2$ (confirming that the spectrum has sufficient signal-to-noise ratio to solve reliably for C, τ). Fig. 12(a) may be compared with fig. 2 of Arav et al. (1999), who carried out a similar analysis, of a Keck spectrum of the mini-BAL in the radio BAL-like quasar 1603+3002. In 1624+3758, the shape of the absorption in the C IV mini-BAL also appears to be dominated by variations with velocity of C rather than variations of τ. For outflow velocities < -2500 km s^{-1}, the optical depth is consistent (within the errors, ≈0.03 in $I_{\rm b}$ and $I_{\rm r}$) with $e^{-\tau} = 0$, i.e. saturated, indicating that the true optical depth is much larger than is implied by the depth of the absorption feature. The limited covering factor $C \sim 0.6$, and the variation of C with velocity, suggest that the mini-BAL is intrinsic to the quasar. The mean covering factor for $v < -2500$ km s^{-1} is ≈0.7 and that for $v > -2500$ km s^{-1} is ≈0.6.

Four effects could complicate the above determination of C and τ for the C IV mini-BAL.

(1) The covering factor of features narrower than the spectral resolution of ISIS (0.8 Å, 36 km s^{-1}) may be underestimated. In particular, the observed absorption minima (FWHM 1.3, 0.9 and 1.5 Å, Fig. 8) might be due to saturated lines of similar equivalent widths. Saturation implies $I_{\rm r}$, $I_{\rm b} = 0$, $C = 1$, $e^{-\tau} = 0$. In addition, inadequate spectral resolution can mimic partial covering, $C < 1$, in the (instrumental) wings of deep absorption features (Ganguly et al. 1999). In the C IV mini-BAL analysed here, absorbers 10 and 11 are separated by five times the instrumental FWHM (0.8 Å), and absorbers 11 and 12 by four times the FWHM, so over most of the wavelength range in these intervals, there should be negligible contamination by the nearby absorption minima. We confirmed this by convolving with the instrumental point-spread function, a simulated spectrum comprising three saturated features (i.e. $C = 1$) at the velocities of absorbers 10, 11 and 12, and with widths 1.0, 0.6 and 0.5 Å (36, 22 and 18 km s^{-1}), respectively, to give the same equivalent widths as observed. The values of $I_{\rm b}$ and $I_{\rm r}$ measured from the convolved spectrum differ from those in the unconvolved spectrum by <0.05, over more than half of the total velocity range $-2300 < v < -2750$ km s^{-1}. This confirms that over most of the resolution elements between the absorption minima, C is smaller than the lower limit on C within the minima, i.e. it supports our conclusion that variations of C dominate the shape of the observed absorption.

(2) The blue component of absorber 10 is blended with the red component of absorber 9 (Fig. 8), so the measured $I_{\rm b} = 0.15$ for the former could be underestimated by up to a few tenths. However, from Fig. 11 it can be seen that given the measured (and unblended) $I_{\rm r} = 0.25$ in the minimum of absorber 10, C at this velocity (-2700 ± 50 Å), is at most overestimated by ∼0.15.

(3) It is assumed above that the BAL clouds cover both the nucleus (continuum) and the broad-emission-line region. If the BAL covers the source of the continuum, but not the BLR (as is perhaps the case for the $z = 3.3498$ absorber in 1624+3758, Section 3.3, and for the mini-BAL/NAL absorber discussed by Arav et al. 1999), then the residual intensities would have to be measured relative to the continuum rather than continuum + BLR. Judging from Fig. 4, the contribution of the BLR at the wavelength of the mini-BAL adds $\gtrsim$15 percent to the light from the continuum, and varies little with

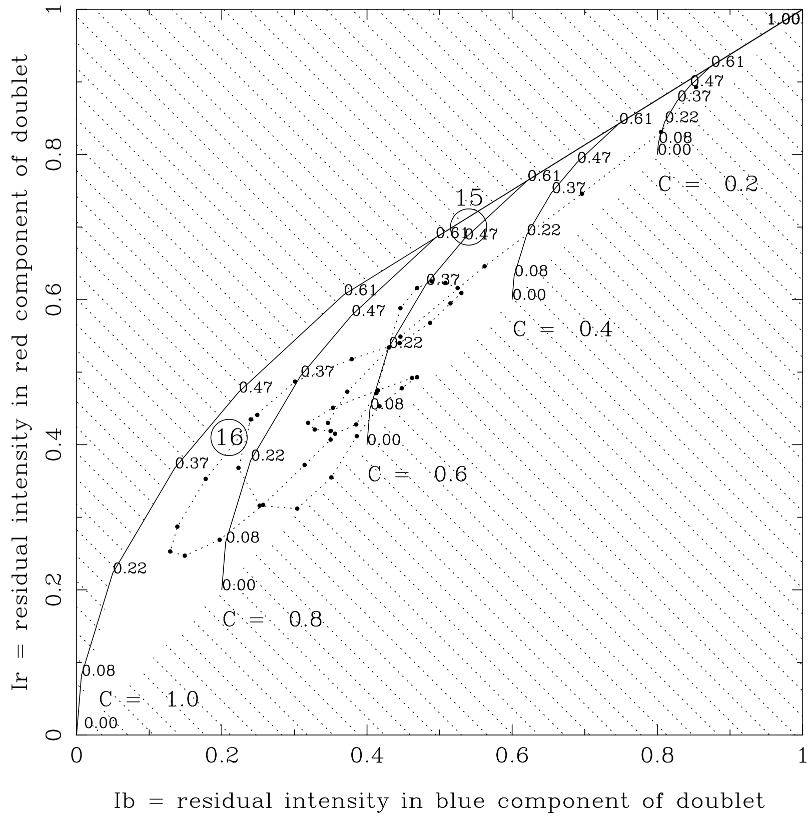

Figure 11. Derivation of the covering factor C and optical depth τ from the residual fractional intensities $I_{\rm b}$, $I_{\rm r}$ in the two components of a doublet with expected optical depth ratio 2:1 (e.g. C IV 1548.2/1550.8 Å, N V 1238.8/1242.8 Å, O VI 1031.9/1037.6 Å). Each solid curve traces for a given covering factor C, the expected variation of $I_{\rm b}$, $I_{\rm r}$ with $e^{-\tau}$. The small numbers on the plot give $e^{-\tau}$ for the blue component of the doublet. Combinations of $I_{\rm b}$, $I_{\rm r}$ in the shaded region of the figure are unphysical (see Section 3.2.1). The dotted curve joins the $I_{\rm b}$, $I_{\rm r}$ values (large dots) measured for the C IV mini-BAL (Fig. 12a) over the velocity range -2730 to -2280 km s^{-1}. The curve lies within the permitted region, confirming that at most velocities the solution for C, $e^{-\tau}$ is well defined. The rms measurement errors on $I_{\rm b}$, $I_{\rm r}$ are $\sim$0.03, and the errors in derived C and $e^{-\tau}$ will be similar. The large circles indicate the values (and rms error radius) of $I_{\rm b}$, $I_{\rm r}$ for the two associated narrow-line C IV absorbers 15 and 16, discussed in Section 3.5.

wavelength across the mini-BAL, so the measured $I_{\rm b}$, $I_{\rm r}$ would have to be revised downwards by $<$0.15 if the mini-BAL does not cover the BLR. This would increase the estimate of the covering factor C by $\approx$0.15, but leaves the estimate of $e^{-\tau}$ almost unchanged.

(4) The equations relating $I_{\rm b}$, $I_{\rm r}$, C and τ are based on the assumption of homogeneous partial coverage, i.e. an opaque screen covering a fraction C of the source. In reality, as emphasized by Hamann & Sabra (2004), absorbers are probably inhomogeneous, with different fractions of the source covered by absorbers of different opacity. However, the modelling of Hamann & Sabra suggests that $e^{-\tau}$ as measured above will typically not differ by more than a few tens of per cent from the true spatially averaged value.

The residual intensities of the blue and red components of absorber 8, just blueward of the other components of the mini-BAL, but probably physically associated, imply a covering factor of $\approx$0.5 and near saturation. No attempt has been made to model the variation of covering factor with velocity, because of blending.

In N V (Fig. 9), the velocity structure is not well resolved (the spectral resolution is poorer, $\approx$130 km s^{-1}), so that a similar analysis (Fig. 12b) tends to underestimate the derived covering factor in the minima, but the mean covering factor $C \sim 0.7$, is similar to that found for C IV and the opacity appears to be less at outflow velocities of -2300 to -2450 km s^{-1}, as for C IV.

A similar analysis in O VI (Figs 10, 12c, same spectral resolution as for N V) is confused by the Lyα forest (and also by Lyβ absorbers 15 and 16). The red component of the O VI doublet due to absorber 10 (which is unconfused by the Lyβ absorption) is black, i.e. the covering factor $C = 1$ and $e^{-\tau} = 0$, in contrast to that for C IV and N V ions. Absorber 11 also appears to have $C \approx 1$. Not much can be said concerning the variation of C and τ with velocity. The poor signal-to-noise ratio in the O VI mini-BAL results in $I_{\rm b} > I_{\rm r}$ (unphysical, see Fig. 11) over some of the velocity range. For these velocities, the plotted curves in Fig. 12(c) give $C = 1 - I_{\rm r}$ and $e^{-\tau} = 0$.

The variation of C with ion (found also by Arav et al. 1999 for 1603+3002) supports the suggestion by Hamann & Sabra (2004) that a given observed covering factor C is often due to inhomogeneous partial coverage, in which the optical depth changes across the source. The stronger transitions can then have $\tau > 1$ over larger areas than weak transitions.

Approximate column densities and limits for the apparently less-saturated part of the mini-BAL (-2300 to -2450 kms^{-1}, $\tau \gtrsim 1$), are given in Table 5. Column-density measurements of this accuracy do not justify detailed photoionization calculations, but the H I, O VI, N V and C IV column densities are consistent with an ionization parameter $\log(U) = -1.5$, $\log N(H_{\rm total}) \sim 18.4$, using the photoionization modelling of Hamann (1997, fig. 2c), with ionizing continuum $F_\nu \propto \nu^{-3/2}$ and meteoritic solar abundances from Grevesse & Anders (1989). The lack of Si IV (and Si II) absorption implies $\log U > -2.0$, i.e. is consistent with the above.

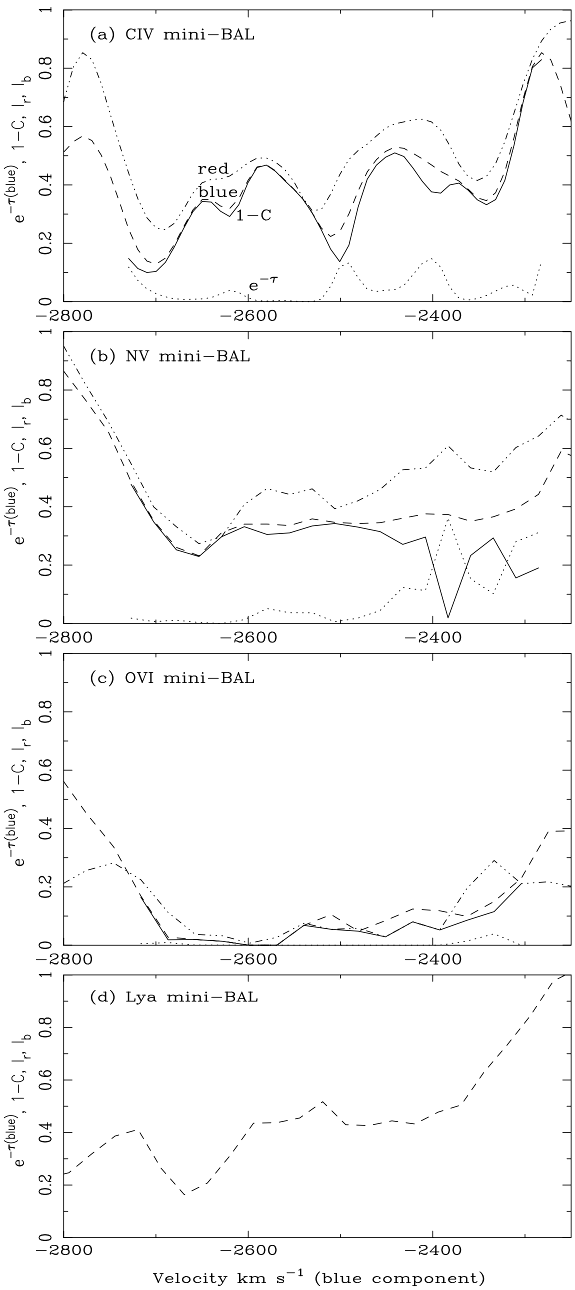

Figure 12. Covering factor C (the solid curve shows $1 - C$) and optical depth $e^{-\tau}$ (in the blue component of the doublet, dotted) derived as a function of velocity for the mini-BAL in (a) C IV, (b) N V and (c) O VI. The residual intensities I_b and I_r from which C and $e^{-\tau}$ were derived are also shown (dashed and dot-dashed curves 'blue' and 'red', respectively). The shape of the C IV mini-BAL is dominated by changes of the covering factor with velocity, rather than by changes in optical depth. C may be overestimated near velocity -2700 km s^{-1} due to blending with absorber 9 (see Section 3.2.1). (d) The Lyα absorption over the same velocity range. The spectral resolution for N V, O VI and Lyα (Figs 12b–d) is a factor of 3 poorer than for C IV (Fig. 12a).

3.2.2 *Possible line-locking*

The C IV mini-BAL comprises five readily identified C IV doublets (absorbers 8–12, Fig. 8). The blue component of the strongest (absorber 10) lies at 6715.8 Å, just 0.2 ± 0.2 Å blue of the 6716.0 expected wavelength of the red component of absorber 9. This suggests that the lines may be locked together. The chance of the red component of a given C IV doublet falling within dλ of the blue component of any other C IV doublet, for N doublets distributed at random over the wavelength range $\Delta\lambda$ is $(d\lambda/\Delta\lambda)N(N-1)/2$. For $\Delta\lambda = 40$ Å, $d\lambda = 0.2$ and $N = 5$, this probability is 0.05, i.e. the above coincidence is moderately significant.

The sixth absorber in the mini-BAL (no 13) was identified in N V only (Fig. 9, expected C IV wavelengths marked in Fig. 8). Interestingly, the red component of the C IV doublet of absorber 10 lies at 6727.1 Å, 0.1 ± 0.2 Å from the 6727.0 Å expected wavelength of the blue component of absorber 13. Absorbers 9, 10 and 13 might therefore be line-locked together (Fig. 8).

Absorption–absorption line-locking can occur when light of the wavelength required for a given transition in one cloud is absorbed by ions in a cloud closer to the quasar, with different velocity and undergoing a different transition. This reduces the radiation force on the shadowed cloud, and the cloud may lock at a velocity difference from the shadowing cloud corresponding to the wavelength difference of the two transitions. In general, several lines will contribute to the total radiation pressure on a cloud, but if this approximates the net force in the opposite direction (gravity and perhaps drag), the effect of line-locking in one line could be significant (Korista et al. 1993). Observation of line-locking lends support to the hypothesis that radiation pressure plays an important role in the acceleration of BAL gas (in at least some quasars). Line-locking is probably seen in the spectra of the $z = 1.8$ quasar 1303+308 (Foltz et al. 1987; Vilkovskij & Irwin 2001) and the $z = 2.9$ quasar 1511+091 (Srianand et al. 2002). The former includes several Si IV absorption doublets spaced by the separation of the two components of the doublet. Plausible examples of line-locking have also been noted in 08279+5255, 1230+0115, 1303+308, 1511+091, 1605−0112 and NGC 5548 (references given in Section 1.1).

3.3 Possible Lyman-limit system at $z = 3.3498$

The absorption feature at 5288 Å (Figs 5, 13 and 14) is flat-bottomed and shows possible damping wings, both suggesting saturation. The feature might be a blend of weaker lines, but here we explore the possibility that this is a saturated Lyα absorber at $z = 3.3498$. The residual flux at the base of the line cannot be due to an intensity-calibration problem, since many of the nearby Lyα-forest lines reach zero intensity. It therefore implies partial coverage of the source,

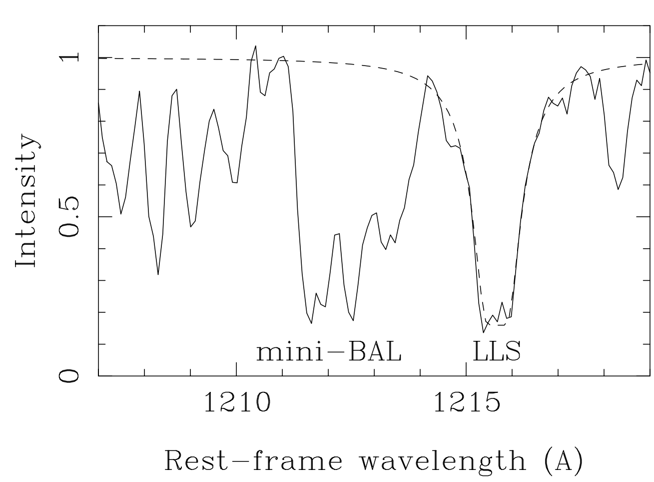

Figure 13. Voigt-profile fit to the $z = 3.3498$ absorber, N(H I) $= 4 \times 10^{18}$ cm^{-2}. No associated metal lines are detected.

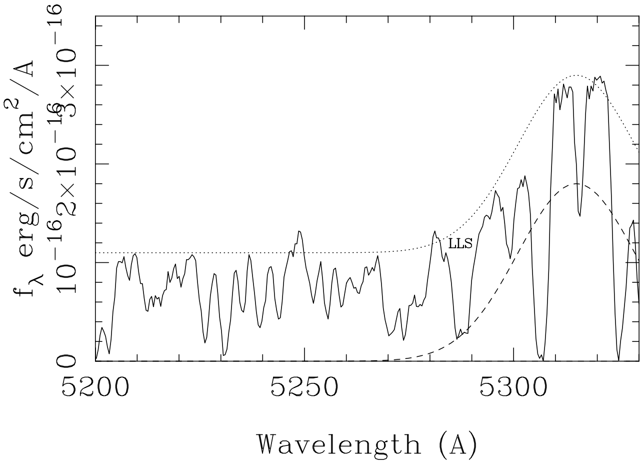

Figure 14. The spectrum of 1624+3758 in the vicinity of the $z = 3.3498$ LLS absorber, showing a possible explanation of the non-black trough. The dotted line is an approximate upper bound to the spectrum blueward of the Lyα emission, and is the sum of a wavelength-independent term (continuum) and a Gaussian of FWHM = 1700 km s^{-1} (dashed line, representing broad Lyα emission). The depth of the $z = 3.3498$ absorption is consistent with the cloud covering the continuum source, but not the broad-line region.

$C = 0.7$. The rest-frame equivalent width of the line is 1.5 Å. A Voigt-profile fit (Fig. 13) yields a column density $N(\mathrm{H\,I}) = 4 \times 10^{18}$ cm^{-2}, velocity parameter $b = 30$ km s^{-1}, i.e. a Lyman-limit system [LLS, $17.2 < \log N(\mathrm{H\,I}) < 20.3$, e.g. Lanzetta, Wolfe & Turnshek 1995].

The corresponding Lyβ falls in a heavily absorbed part of the Lyα forest, but may be detected, with the expected rest-frame equivalent width ∼1.0 Å. The Lyman limit would be at 3967 Å, but the SDSS spectrum has zero intensity bluewards of 3980 Å, perhaps due to Lyman-limit absorption by absorber 15 (see Section 3.5). Surprisingly, no metal lines are detected, $N(\mathrm{Si\,II})$, $N(\mathrm{Si\,IV})$, $N(\mathrm{C\,IV}) \gtrsim 10^{13}$ cm^{-2}. This cannot be due to very high ionization, because no combination (Hamann 1997) of ionization parameter $\log U > 0$ and $N(\mathrm{H}) < 10^{24}$ cm^{-2} (above which the gas would be Thomson-thick) is consistent with the observed limits on metal column density. It might be due to low metallicity, which is one possible interpretation of the lack of metal lines in another non-black absorber: that found by Petitjean & Srianand (1999) in the $z = 2.2$ quasar J2233−606, with $\log N(\mathrm{H\,I}) = 14$ and $C = 0.7$.

The limited covering factor, $C < 1$, implies that the putative absorber is intrinsic, and close to the nucleus of the quasar. The mini-BAL (Section 3.2) has a similar covering factor, which might indicate a similar physical location. Alternatively, the absorber might be covering the quasar continuum source only and not the broad-line region (Fig. 14).

3.4 BAL ($2.968 < z < 3.085$)

The C IV BAL extends over observed wavelengths 6150–6330 Å, outflow velocity −29 300 to −20 700 km s^{-1}. It is also detected in N V and Si IV, and perhaps in Lyα (see Figs 4 and 5), although the Si IV trough is partially masked by the broad Lyα and O I emission. The BALnicity index of 1624+3758 is 2990 km s^{-1}. The BAL turns on and off over ≈700 km s^{-1}. The feature bisecting the BAL at 6232 Å corresponds to no known emission line, and is probably just a gap in the velocity structure. The mean depth of the BAL is 0.35 times the intensity of the continuum. BALs are usually saturated (Hamann, Korista & Morris 1993), so the observed depth implies a covering factor of 0.35. The observed spectrum is consistent with a similar covering factor in N V and Si IV.

The BAL is not detected in absorption in the Al III (1855, 1863 Å) doublet (expected wavelengths 7373–7590 Å; see Fig. 4), suggesting that the quasar is a HiBAL (but see Section 4).

3.5 Narrow C IV absorption features

In addition to the absorbers discussed above, nine C IV NALs are detected (Table 4).

The C IV lines of absorbers 15 and 16 are deep, and have small velocities relative to the quasar (> −1000 km s^{-1}). They are thus likely to be physically associated with the quasar. Absorber 16 is slightly redshifted relative to the emission-line redshift of the quasar, but by only one standard deviation. Both absorbers are resolved in velocity. The residual intensities in the blue and red components are consistent with a covering factor of $C = 1$ (Fig. 11), and moderate optical depth. The Lyα lines of both absorbers are saturated, with a rest-frame equivalent width of ≈0.8 Å, implying $N(\mathrm{H\,I}) < 10^{18}$ cm^{-2}. The Lyβ lines are probably detected (Fig. 10), but are confused by the O VI mini-BAL. The Lyman limits for these two absorbers would fall at wavelengths 3981 and 3995 Å. The SDSS spectrum shows zero intensity below 3980 Å, so absorber 15 may be a Lyman-limit system [LLS, $\log N(\mathrm{H\,I}) > 17.2$].

The remaining narrow C IV lines (1–7), with $v < -5000$ km s^{-1}, are likely to be intervening absorbers, physically unrelated to the quasar. Misawa et al. (2002) measured the number density per unit redshift, $n(z)$, of intervening C IV absorbers. Combining their results with those of Steidel (1990), the mean $n(z) = 2 \pm 1$ at $z \sim 3$, for rest-frame equivalent width EW > 0.15 Å in both components of the doublet. For 1624+3758, we find three C IV doublets satisfying these criteria (absorbers 1, 2, 7) over a redshift range of 0.7, i.e. 4.3 ± 2 per unit redshift, not significantly different from that found by Misawa et al. and and Steidel [and contrasting with the much higher $n(z) = 7$ found for 0747+2739, Richards et al. 2002a]. Of the absorbers noted here, 4, 6 and 7 are slightly resolved in velocity (Table 3), consistent with the internal velocity dispersions typical of normal galaxies, ∼50 km s^{-1}. The rms errors on the equivalent widths in the blue and red components of each doublet (absorbers 1–7) are large, but the measurements are consistent with a covering factor of $C = 1$, as expected for absorbers for which the physical dimensions greatly exceed those of the emitting region.

Most of the NALs are detected in Lyα and several in Lyβ (Figs 5 and 10). None of the NALs is detected in absorption by O I (1302.17 Å), Si II (1526.71 Å), Fe II (1608.45 Å), Al II (1670.79 Å) or Al III (1854.72 Å).

4 THE NATURE OF 1624+3758

The lack of detectable BAL absorption in the Al III doublet (Section 3.4) suggests that the quasar is a HiBAL, but the observed spectrum does not extend to Mg II 2800 Å, so it could also be an atypical LoBAL with weak Al III absorption. The O I equivalent width and the presence of Fe II/Fe III emission (Section 3.1) are typical of LoBALs, as is the continuum colour (although this also falls within the range of colours of HiBALs). The frequency of LoBALs amongst radio BAL quasars appears to be twice as high (∼30 per cent; Becker et al. 2000, 2001; Menou et al. 2001) as amongst non-radio BAL quasars (∼15 per cent).

Regardless of whether the quasar is a HiBAL or a LoBAL, the Fe II UV191 triplet emission line at 1787 Å (and Fe III at 1896/1914 Å) is unusually strong (Section 3.1). The association of unusually high radio luminosity (Section 1.2) and unusually strong Fe II emission suggests a connection between the two. Such a connection is also suggested by the fact that the 1787-Å line is detectable in only one out of 40 SDSS BAL quasars with no FIRST counterparts, but in four out of 14 of the SDSS BAL quasars with $S_{1.4\,\mathrm{GHz}} > 1$ mJy (Section 3.1). Boroson (2002) and Lamy & Hutsemekers (2004) note that strong Fe II emission might be a signature of the thickening of the accretion disc at accretion rates close to the Eddington limit, $L/L_{\mathrm{edd}} \sim 1$. Although the intensity of this 'small blue bump' Fe II emission might not always be proportional to that of the Fe II 1787-Å line (Vestergaard & Wilkes 2001), it is plausible that the unusually strong Fe II 1787-Å emission in 1624+3758 is related to the very high accretion rates posited for radio BAL quasars (Boroson 2002).

The detachment of the BAL by 21 000 km s^{-1} from the C IV emission line is moderately unusual, being observed in ∼10 per cent of BAL quasars with either $z < 3$ or $z > 3$. It suggests an angle of view well away from the plane of the accretion disc, so that the line of sight to the quasar nucleus exits the curving streamlines far above the disc (see fig. 8 of Lamy & Hutsemekers 2004).

The radio rotation measure of 1624+3758 is the second largest known. It is due to the properties of gas lying between us and the radio-emitting region (size $\gtrsim$ 1 kpc), and is unlikely to depend strongly on orientation. It implies a high value of at least one of the magnetic field, electron density or path-length through the region responsible.

In summary, the observed properties of the quasar are more consistent with it being intrinsically unusual than with it being viewed at an unusual orientation. 1624+3758 is highly radio-luminous, and it may be a good example of an object which is accreting both at a very high rate (high $\mathrm{d}M/\mathrm{d}t$) and near the Eddington limit.

5 CONCLUSIONS

We report high-resolution spectroscopy and radio observations of the BAL quasar 1624+3758, $z = 3.377$. 1624+3758 is the most radio-luminous BAL quasar known, $P_{1.4\,\mathrm{GHz}} = 4.3 \times 10^{27}$ W Hz^{-1}. It is also highly luminous in the optical, $M_{AB}(1450\,\mathrm{Å}) \approx -27.6$, luminosity $L_{1450} \sim 5 \times 10^{24}$ W Hz^{-1}.

(1) The Fe II UV191 1787-Å emission triplet is unusually prominent, rest-frame EW = 3.8 Å. Fe III UV34 1896/1914 Å is also detected.

(2) The BAL has BALnicity index BI = 2990 km s^{-1}, outflow velocity −21 000 to −29 000 km s^{-1}. The large detachment velocity suggests an angle of view well away from the plane of the accretion disc.

(3) A complex mini-BAL is detected in C IV, N V and O VI, with velocity −2200 to −3400 km s^{-1}. For C IV, we have measured the covering factor and optical depth as a function of velocity −2300 to −2700 km s^{-1}. The shape of the absorption is dominated by the variation with velocity of the covering factor. This variation implies that the mini-BAL is intrinsic to the quasar.

(4) There is statistical evidence of line-locking between two (and perhaps three) of the mini-BAL absorption components, supporting the hypothesis that the outflows are accelerated by radiation pressure.

(5) A possible non-black H I absorber is observed with velocity −1870 km s^{-1}, $N(\mathrm{H\,I}) = 4 \times 10^{18}$ cm^{-2} (LLS). There are no associated metal lines. The covering factor is only 0.7, suggesting that the absorber is intrinsic to the quasar, perhaps covering the continuum source, but not the broad-line region.

(6) The velocities relative to the quasar of two of the C IV NALs are small (−824, 206 km s^{-1}). They are likely to be intrinsic. The other seven NALs ($v < -5000$ km s^{-1}) are probably intervening systems. The number density of C IV absorbers with $v < -5000$ km s^{-1} and rest-frame equivalent width EW > 0.15 Å, is $n(z) = 4.3 \pm 2$, consistent with that measured for other quasars.

(7) The wings of the C IV and N V emission lines are markedly asymmetric, consistent with the red wings being suppressed, perhaps due to dust extinction of light emitted by gas outflows on the far side of the nucleus.

(8) The width of the C IV emission line, in conjunction with the optical luminosity L, implies a black hole mass $M_{\mathrm{BH}} \sim 10^9\,\mathrm{M}_\odot$ and $L/L_{\mathrm{Eddington}} \sim 2$.

(9) The radio spectrum turns over at rest frame ∼2 GHz, suggestive of a young compact source. The source is slightly resolved by the VLA observation, projected size ∼2.8 kpc.

(10) The radio source is 11 per cent polarized at 10 GHz and the rest-frame rotation measure, 18 350 rad m^{-2} is the second highest known for any extragalactic source.

(11) The conjunction of several unusual features, particularly the strong Fe II 1787-Å emission and the high radio rotation measure, favour the quasar being intrinsically unusual rather than being viewed at an unusual orientation. Given the high radio luminosity, the unusual features may be due to a combination of a very high accretion rate and high $L/L_{\mathrm{Eddington}}$, i.e. this quasar may occupy an extreme position in Boroson's (2002) classification scheme for AGN.

ACKNOWLEDGMENTS

We are grateful to Pierre Leisy for obtaining one of the spectra during WHT service time, to Marek Jamrozy for making the Effelsberg observations and to the anonymous referee for helpful suggestions. CRB, RC, MV and JIGS acknowledge financial support from the Spanish Ministerio de Ciencia y Tecnologí a under project AYA2002-03326. The William Herschel Telescope is operated on the island of La Palma by the Isaac Newton Group in the Spanish Observatorio del Roque de Los Muchachos of the Instituto de Astrofisica de Canarias. The 100-m Effelsberg radio telescope is operated by the Max Planck Institut für Radioastronomie. The National Radio Astronomy Observatory is operated by Associated Universities, Inc., under cooperative agreement with the National Science Foundation. The Westerbork Synthesis Radio Telescope (WSRT) is operated by the Netherlands Foundation for Research in Astronomy (ASTRON) with financial support of the Netherlands Organization for Scientific Research (NWO). The Two Micron All-sky Survey is a joint project of the University of Massachusetts and the Infrared Processing and Analysis Centre/California Institute of Technology, funded by NASA and the NSF. The Sloan Digital Sky Survey is funded by the Alfred P. Sloan foundation, the SDSS member institutions, NASA, NSF, the US Department of Energy, the Japanese Monbukagakusho and the Max Planck Society.

REFERENCES

Abazajian K. et al., 2005, AJ, 129, 1755
Arav N., Becker R. H., Laurent-Muehleisen S. A., Gregg M. D., White R. L., Brotherton M. S., de Kool M., 1999, ApJ, 524, 566
Arav N. et al., 2001, ApJ, 561, 118
Arav N., Korista K. T., de Kool M., 2002, ApJ, 566, 699
Baars J. W. M., Genzel R., Pauliny-Toth I. I. K., Witzel A., 1977, A&A, 61, 99

Barlow T. A., Sargent W. L. W., 1997, AJ, 113, 136
Barlow T. A., Hamann F., Sargent W. L. W., 1997, in Arav N., Shlosman I., Weymann R. J., eds, ASP Conf. Ser. Vol. 128, Mass Ejection from Active Galactic Nuclei. Astron. Soc. Pac., San Francicso, p. 13
Becker R. H., White R. L., Gregg M. D., Brotherton M. S., Laurent-Muehleisen S. A., Arav N., 2000, ApJ, 538, 72
Becker R. H. et al., 2001, ApJS, 135, 227
Benn C. R., Vigotti M., Pedani M., Holt J., Mack K.-H., Curran R., Sánchez S. F., 2002, MNRAS, 329, 221
Blustin A. J., Page M. J., Fuerst S. V., Branduardi-Raymont G., Ashton C. E., 2005, A&A, 431, 111
Boroson T., 2002, ApJ, 565, 78
Boroson T., Meyers K. A., 1992, ApJ, 397, 442
Briggs F. H., Turnshek D. A., Wolfe A. M., 1984, ApJ, 287, 549
Brotherton M. S., van Breugel W., Smith R. J., Boyle B. J., Shanks T., Croom S. M., Miller L., Becker R. H., 1998, ApJ, 505, L7
Brotherton M. S., Croom S. M., De Breuck C., Becker R. H., Gregg M. D., 2002, AJ, 124, 2575
Churchill C. W., Schneider D. P., Schmidt M., Gunn J. E., 1999, AJ, 117, 2573
Condon J. J., Cotton W. D., Greisen E. W., Yin Q. F., Perley R. A., Taylor G. B., Broderick J. J., 1998, AJ, 115, 1693
Crenshaw D. M., Kraemer S. B., George I. M., 2002, Mass outflow in AGN: new perspectives. ASP Conf. Ser. Vol. 255. Astron. Soc. Pac., San Francisco
Cutri R. M. et al., 2003, CDS/ADC collection of electronic catalogues, 2246
de Kool M., 1997, in Arav N., Shlosman I., Weymann R. J., ASP Conf. Ser. Vol. 128, Mass Ejection from Active Galactic Nuclei. Astron. Soc. Pac., San Francisco, p. 233
de Kool M., Arav N., Becker R. H., Gregg M. D., White R. L., Laurent-Muehleisen S. A., Price T., Korista K. T., 2001, ApJ, 548, 609
D'Odorico V., Cristiani S., Romano D., Granato G. L., Danese L., 2004, MNRAS, 351, 976
Elvis M., 2000, ApJ, 545, 63
Fabian A. C., 1999, MNRAS, 308, L39
Foltz C. B., Weymann R. J., Morris S. L., Turnshek D. A., 1987, ApJ, 317, 450
Ganguly R., Eracleous M., Charlton J. C., Churchill C. W., 1999, AJ, 117, 2594
Ganguly R., Masiero J., Charlton J. C., Sembach K. R., 2003, ApJ, 598, 922
Gaskell C. M., 1982, ApJ, 263, 79
Graham M. J., Clowes R. G., Campusano L. E., 1996, MNRAS, 279, 1349
Gregg M. D., Becker R. H., Brotherton M. S., Laurent-Muehleisen S. A., Lacy M., White R. L., 2000, ApJ, 544, 142
Grevesse N., Anders E., 1989, in Waddington C. I., ed., AIP Conf. Proc. 183, Cosmic Abundances of Matter. AIP, New York, p. 1
Gupta N., Srianand R., Petitjean P., Ledoux C., 2003, A&A, 406, 65
Hall P. B. et al., 2002, ApJS, 141, 267
Hall P. B., Hutsemekers D., Anderson S. F., Brinkmann J., Fan X., Schneider P., York D. G., 2003, 593, 189
Hamann F., 1997, ApJS, 109, 279
Hamann F., Sabra B., 2004, in Richards G. T., Hall P. B., ASP Conf. Ser. Vol. 311, AGN Physics with the Sloan Digital Sky Survey. Astron. Soc. Pac., San Francisco, p. 203
Hamann F., Korista K. T., Morris S. L., 1993, ApJ, 415, 541
Hamann F., Barlow T. A., Junkkarinen V., Burbidge E. M., 1997, ApJ, 478, 80
Hartig G. F., Baldwin J. A., 1986, ApJ, 302, 64
Hewett P. C., Foltz C. B., 2003, AJ, 125, 1784
Holt J., Benn C. R., Vigotti M., Pedani M., Carballo R., Gonzalez-Serrano J. I., Mack K.-H., Garcia B., 2004, MNRAS, 348, 857
Hutsemékers D., Hall P. B., Brinkmann J., 2004, A&A, 415, 77
Jaffe W. J., Perola G. C., 1973, A&A, 26, 423
Jannuzi B. T. et al., 1996, ApJ, 470, L11
Kaspi S., Smith P. S., Netzer H., Maoz D., Jannuzi B. T., 2000, ApJ, 533, 631
Kassim N. E., Lane W. M., Cohen A. S., Lazio T. J. W., Perley R. A., Cotton W. D., Condon J. J., Erickson W. C., 2003, A&AS, 203, 5709
Kato T., Tabara H., Inoue M., Aizu K., 1987, Nat, 329, 223
Korista K. T., Voit G. M., Morris S. L., Weymann R. J., 1993, ApJS, 88, 357
Lacy M., Laurent-Muehleisen S. A., Ridgway S. E., Becker R. H., White R. L., 2001, ApJ, 551, L17
Lamy H., Hutsemekers D., 2004, A&A, 427, 107
Lanzetta K. M., Wolfe A. M., Turnshek D. A., 1995, ApJ, 440, 435
Lewis G. F., Chapman S. C., Kuncic Z., 2003, ApJ, 596, L35
Maiolino R., Oliva E., Ghinassi F., Pedani M., Mannucci F., Mujica R., Juarez Y., 2004, A&A, 420, 889
Menou K. et al., 2001, ApJ, 561, 645
Miley G., 1980, ARA&A, 18, 165
Misawa T., Tytler D., Iye M., Storrie-Lombardi L. J., Suzuki N., Wolfe A. M., 2002, AJ, 123, 1847
Morton D. C., 2003, ApJS, 149, 205
Murgia M., Fanti C., Fanti R., Gregorini L., Klein U., Mack K.-H., Vigotti M., 1999, A&A, 345, 769
Murray N., Chiang J., Grossman S. A., Voit G. M., 1995, ApJ, 451, 498
O'Dea C. P., 1998, PASP, 110, 493
Osterbrock D. E., Fulbright J. P., Martel A. R., Keane M. J., Trager S. C., Basri G., 1996, PASP, 108, 277
Pacholczyk A. G., 1970, Radio Astrophysics. Freeman, San Francisco
Pei Y. C., 1992, AJ, 395, 130
Petitjean P, Srianand R., 1999, A&A, 345, 73
Reichard T. A. et al., 2003a, AJ, 125, 1711
Reichard T. A. et al., 2003b, AJ, 126, 2594
Reichard T. A., Richards G. T., Hall P. B., Schneider D. P., 2004, in Richards G. T., Hall P. B., eds, ASP Conf. Ser. Vol. 311, AGN Physics with the Sloan Digital Sky Survey. Astron. Soc. Pac., San Francisco, p. 219
Rengelink R. B., Tang Y., de Bruyn A. G., Miley G. K., Bremer M. N., Röttgering H. J. A., Bremer M. A. R., 1997, A&AS, 124, 259
Richards G. T., Gregg M. D., Becker R. H., White R. L., 2002a, ApJ, 567, L13
Richards G. T., vanden Berk D. E., Reichard T. A., Hall P. B., Schneider D. P., SubbaRao M., Thakar A. R., York D. G., 2002b, AJ, 124, 1
Savage B. D., Sembach K. R., 1991, ApJ, 379, 245
Silk J., Rees M. J., 1998, A&A, 331, L1
Srianand R., Petitjean P., 2000, A&A, 357, 414
Srianand R., Petitjean P., 2001, A&A, 373, 816
Srianand R., Petitjean P., Ledoux C., Hazard C., 2002, MNRAS, 336, 753
Steidel C. C., 1990, ApJS, 72, 1
Stocke J., Morris S. L., Weymann R. J., Foltz C. B., 1992, ApJ, 396, 487
Tolea A., Krolik J. H., Tsvetanov Z., 2002, ApJ, 578, L31
Tytler D., Fan X.-M., 1992, ApJS, 79, 1
Vanden Berk D. E. et al., 2001, AJ, 122, 549
Verner D. A., Barthel P. D., Tytler D., 1994, A&AS, 108, 287
Vestergaard M., Wilkes B., 2001, ApJS, 134, 1
Vigotti M., Gregorini L., Klein U., Mack K.-H., 1999, A&AS, 139, 359
Vilkovskij E. Y., Irwin M. J., 2001, MNRAS, 321, 4
Warner C., Hamann F., Dietrich M., 2004, ApJ, 608, 136
Weymann R. J., Morris S. L., Foltz C. B., Hewett P. C., 1991, ApJ, 373, 23
White R. L., Becker R. H., Helfand D. J., Gregg M. D., 1997, ApJ, 475, 479
Willott C., Rawlings S., Grimes J. A., 2003, ApJ, 598, 909
Wise J. H., Eracleous M., Charlton J. C., Ganguly R., 2004, ApJ, 613, 129
York D. G. et al., 2000, AJ, 120, 1579
Zavala R. T., Taylor G. B., 2004, ApJ, 612, 749

This paper has been typeset from a TEX/LATEX file prepared by the author.